Location of largest earthquake slip and fast rupture controlled by along-strike change in fault structural maturity due to fault growth

C. Perrin, I. Manighetti, J.-P. Ampuero, F. Cappa, Y. Gaudemer

AGU PUBLICATIONS

JGR

Journal of Geophysical Research: Solid Earth

RESEARCH ARTICLE

10.1002/2015JB012671

Key Points:
- Earthquake slip asymmetry relates to along-strike changes in fault properties due to fault growth
- Largest slip and faster rupture speed systematically occur on most mature half of ruptured fault sections
- Larger slip is promoted by greater off-fault compliance and lower fault strength in mature parts

Supporting Information:
- Supporting Information S1
- Table S1
- Figure S1
- Figure S2

Correspondence to:
C. Perrin,
cperrin@ldeo.columbia.edu

Citation:
Perrin, C., I. Manighetti, J.-P. Ampuero, F. Cappa, and Y. Gaudemer (2016), Location of largest earthquake slip and fast rupture controlled by along-strike change in fault structural maturity due to fault growth, *J. Geophys. Res. Solid Earth*, *121*, 3666–3685, doi:10.1002/2015JB012671.

Received 19 NOV 2015
Accepted 28 APR 2016
Accepted article online 1 MAY 2016
Published online 20 MAY 2016

Location of largest earthquake slip and fast rupture controlled by along-strike change in fault structural maturity due to fault growth

Clément Perrin[1,2], Isabelle Manighetti[1], Jean-Paul Ampuero[3], Frédéric Cappa[1,4], and Yves Gaudemer[5]

[1]Université Nice Sophia Antipolis, Géoazur (UMR7329), CNRS, Observatoire de la Côte d'Azur, Sophia-Antipolis, France, [2]Now at Lamont-Doherty Earth Observatory, Columbia University, New York, New York, USA, [3]Seismological Laboratory, California Institute of Technology, Pasadena, California, USA, [4]Institut Universitaire de France, Paris, France, [5]Institut de Physique du Globe de Paris, Sorbonne Paris Cité, Paris VII–Denis Diderot University, CNRS, Paris, France

Abstract Earthquake slip distributions are asymmetric along strike, but the reasons for the asymmetry are unknown. We address this question by establishing empirical relations between earthquake slip profiles and fault properties. We analyze the slip distributions of 27 large continental earthquakes in the context of available information on their causative faults, in particular on the directions of their long-term lengthening. We find that the largest slips during each earthquake systematically occurred on that half of the ruptured fault sections most distant from the long-term fault propagating tips, i.e., on the most mature half of the broken fault sections. Meanwhile, slip decreased linearly over most of the rupture length in the direction of long-term fault propagation, i.e., of decreasing structural maturity along strike. We suggest that this earthquake slip asymmetry is governed by along-strike changes in fault properties, including fault zone compliance and fault strength, induced by the evolution of off-fault damage, fault segmentation, and fault planarity with increasing structural maturity. We also find higher rupture speeds in more mature rupture sections, consistent with predicted effects of low-velocity damage zones on rupture dynamics. Since the direction(s) of long-term fault propagation can be determined from geological evidence, it might be possible to anticipate in which direction earthquake slip, once nucleated, may increase, accelerate, and possibly lead to a large earthquake. Our results could thus contribute to earthquake hazard assessment and Earthquake Early Warning.

1. Introduction

The spatial distribution of earthquake slip is heterogeneous at various length scales and is often described as a stochastic field [e.g., *Bouchon*, 1997; *Mai and Beroza*, 2002; *Liu-Zeng et al.*, 2005; *Lavallée et al.*, 2006]. However, at the largest scales earthquake slip distributions have generic features: independent of slip mode, magnitude, and tectonic setting, envelopes of earthquake slip profiles along strike are characterized by a pronounced asymmetry and a fairly linear decrease over a long section of the rupture, leading on average to an asymmetric triangular slip profile [*Scholz and Lawler*, 2004; *Manighetti et al.*, 2005; *Wesnousky*, 2008] (see Figure 3 further below). Although this systematic asymmetry of earthquake slip is well documented for large earthquakes ($M_w \geq$~6), its origin is not yet understood. Here we address this open question by developing empirical relations between large-scale asymmetry of earthquake slip and fault structural properties and by investigating their connections to the physics of the rupture process and fault growth.

Earthquake slip asymmetry is a generic feature, and therefore, our objective here is to identify the deterministic, generic factors that might control it. Slip heterogeneity may arise from heterogeneities of stress or material properties, including fault friction properties, fluid-related fault zone properties, and elastic stiffness of the host rock [e.g., *Nur*, 1978; *Israel and Nur*, 1979; *Madariaga*, 1979; *Bürgmann et al.*, 1994]. Prior studies have shown that certain structural properties of faults affect significantly the properties of the earthquakes they host, such as their slip amplitude and rupture length [*Manighetti et al.*, 2007], magnitude [*Anderson et al.*, 1996], magnitude-frequency distribution [*Stirling et al.*, 1996], apparent stress drop [*Cao and Aki*, 1986; *Choy and Kirby*, 2004; *Manighetti et al.*, 2007; *Hecker et al.*, 2010], number of broken segments [*Wesnousky*, 1988; *Manighetti et al.*, 2007], and ground motion amplitudes [*Radiguet et al.*, 2009]. *Scholz and Lawler* [2004] and *Manighetti et al.* [2005] suggested that linear earthquake slip profiles imply off-fault coseismic inelastic deformation, referred to as "coseismic damage." *Cappa et al.* [2014] showed, through 3-D dynamic rupture simulations, that asymmetric triangular earthquake slip profiles are produced by faults embedded in a permanent damage

zone whose compliance varies along strike. These findings indicate that properties of both the faults and their embedding medium might significantly affect earthquake slip distributions.

Here we examine which geological properties of faults might control the generic envelope of earthquake slip distributions. In section 2, we define the qualitative concept of fault structural maturity, which we use later to propose a unified interpretation of our observations. In section 3, we describe our compilation of slip distributions of about 30 large (M_w 6.5–8.1) well-documented continental earthquakes of various slip modes and locations worldwide, estimates of rupture speeds for 12 of them, maps of their causative faults, and information on their long-term lateral growth (1–60 Ma). In section 4, we show that although some of the data are inherently qualitative and uncertain, they reveal general trends: the largest earthquake slips and faster rupture speeds are systematically located on the portions of rupture lying on fault sections that formed earlier, and the fairly linear decrease of earthquake slip with distance occurs in the direction of long-term fault propagation. In section 5, we discuss our observations in relation with fault structural maturity and with earthquake physics.

2. Structural Maturity: A Multivariate Fault Property That Changes in Time and Space

Long-term fault growth by lengthening (i.e., lateral propagation) has been observed on natural faults [e.g., *Jackson et al*., 1996; *Burbank et al*., 1996; *Manighetti et al*., 1997, 1998, 2001a, 2001b; *Meyer et al*., 1998; *Vermilye and Scholz*, 1998; *Armijo et al*., 1999; *Keller et al*., 1999; *Ferrill et al*., 1999; *Childs et al*., 2003; *Chen et al*., 2007; *Aydin and Berryman*, 2010; *Faulkner et al*., 2011], modeled experimentally [e.g., *Moore and Lockner*, 1995; *Mansfield and Cartwright*, 2001; *Otsuki and Dilov*, 2005; *Schlagenhauf et al*., 2008] and theoretically [e.g., *Segall and Pollard*, 1983; *Cowie and Scholz*, 1992b; *Bürgmann et al*., 1994; *Du and Aydin*, 1995; *Martel*, 1997; *Davatzes and Aydin*, 2003; *D'Alessio and Martel*, 2004; *Willson et al*., 2007; *Mutlu and Pollard*, 2008], and inferred from the empirical scaling relations between fault length and total accumulated displacement (or "net slip") [e.g., *Walsh and Watterson*, 1988; *Marrett and Allmendinger*, 1990; *Cowie and Scholz*, 1992a; *Dawers et al*., 1993; *Cartwright et al*., 1995; *Schlische et al*., 1996; *Manighetti et al*., 2001a]. While slip accumulation on a fault mainly occurs during earthquakes, fault lengthening is an episodic process that recurs every multiple seismic cycles [e.g., *Childs et al*., 2003; *Nicol et al*., 2005, 2010; *Bull et al*., 2006; *Schlagenhauf et al*., 2008; *Meyer et al*., 1998; *Giba et al*., 2012; *Manighetti et al*., 2015]. Fault propagation rates, averaged over the entire fault lifetime, are up to several cm/yr [*Mueller and Talling*, 1997; *Manighetti et al*., 1997, 1998, 2001b; *Meyer et al*., 1998; *Armijo et al*., 1999; *Keller et al*., 1998, 1999; *Morewood and Roberts*, 1999; *Jackson et al*., 2002; *Childs et al*., 2003; *Hubert-Ferrari et al*., 2003; *Bennett et al*., 2005, 2006; *Chen et al*., 2007].

A qualitative definition of the "structural maturity" of a fault is the degree of advancement in the evolution of its structural properties. If the structural evolution of a fault were rate independent and driven only by the total deformation it accommodates (i.e., if a fast fault and a slow fault reach identical structural states, but at different times), fault maturity could be quantified by the net slip accumulated over the fault lifetime, as commonly done [e.g., *Wesnousky*, 1988; *Stirling et al*., 1996; *Choy and Kirby*, 2004; *Choy et al*., 2006; *Scholz*, 2006; *Sagy et al*., 2007; *Hecker et al*., 2010; *Niemeijer et al*., 2010; *Malagnini et al*., 2010; *Wechsler et al*., 2010; *Ikari et al*., 2011; *Dolan and Haravitch*, 2014]. However, the competition between damage and healing processes may introduce rate dependency in the evolution of fault structure (i.e., a slow fault may heal more than a fast fault and hence reach a similar structural state at larger net slip), and hence, fault age and slip rate are also potentially relevant proxies for structural maturity. Since faults lengthen over their lifetime, their length can also be considered as a proxy for their maturity. In practice, following *Manighetti et al*. [2007], we classify fault structural maturity through a combination of four interrelated fault parameters that are potentially observable: initiation age (I-Age), net slip (D_{Total}), length (L), and slip rate (MR). *Manighetti et al*. [2007] classify faults into "mature faults" ($L \geq 1000$ km and/or I-Age ≥ 10 Ma and/or MR ~ a few cm/yr and/or $D_{\text{Total}} \geq 100$ km), "immature faults" ($L < 300$ km and/or I-Age < a few Ma and/or MR < 1 cm/yr and/or $D_{\text{Total}} < 10$ km), and faults of "intermediate maturity" ($300 \leq L < 1000$ km and/or $5 <$ I-Age < 10 Ma and/or MR ~ 1 cm/yr and/or D_{Total} ~ a few tens of kilometers). Although this classification contains subjective choices, it is based on more information than age or net slip alone and can be applied to most faults worldwide. We will thus use it in the following. The structural maturity defined in that way describes a fault globally, over its entire length and lifetime, and therefore we call it the "overall maturity."

Fault lengthening induces a pattern of decreasing age and decreasing cumulative slip along the fault in its direction(s) of lateral propagation. A manifestation of this pattern is the typical linear tapering of net slip

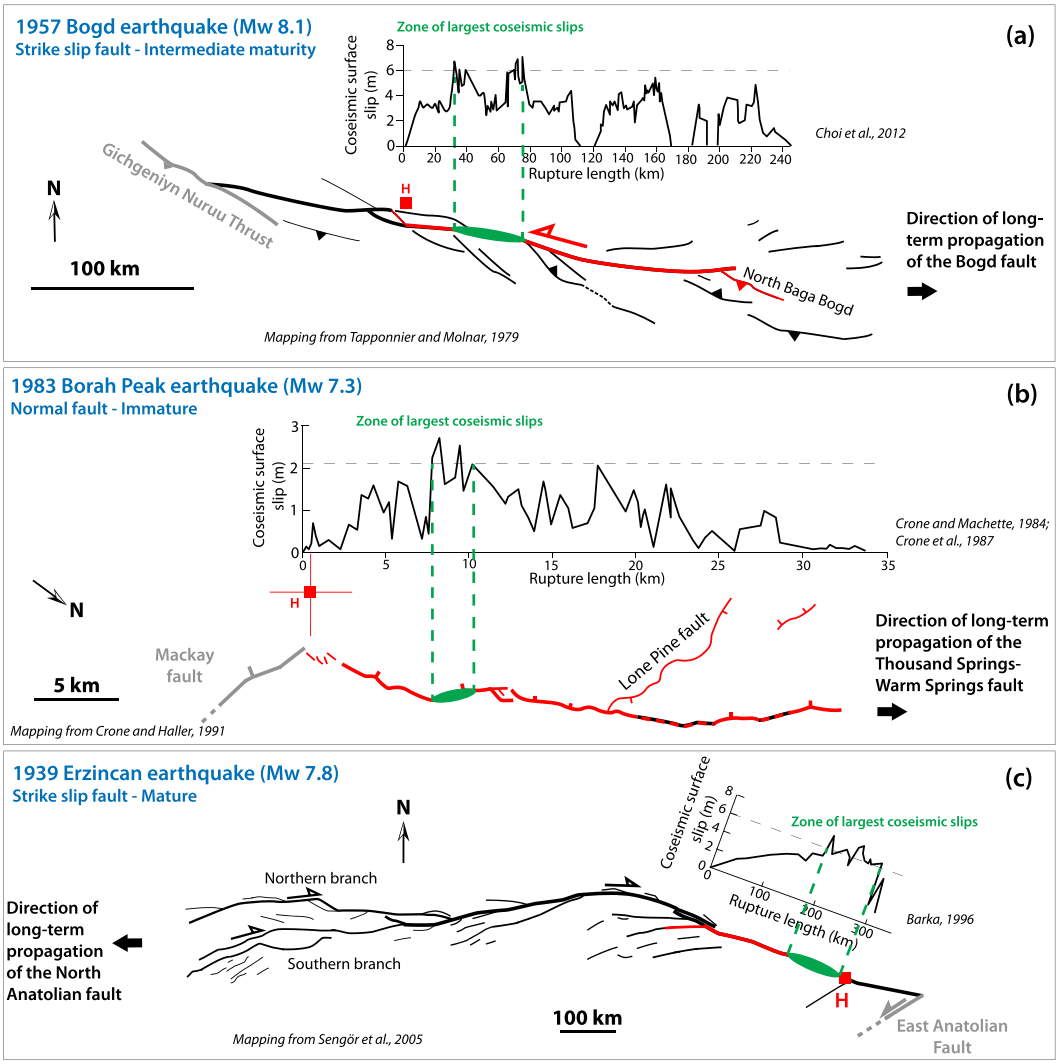

Figure 1. Earthquake examples showing relations between surface rupture trace and slip, and architecture and long-term propagation of causative fault (all earthquakes shown in Figure S1). (a) 1957 M_w 8.1 Bogd, (b) 1983 M_w 7.3 Borah Peak, (c) 1939 M_w 7.8 Erzincan, (d) 1999 M_w 7.4–7.6 Izmit, (e) 2005 M_w 7.6 Muzaffarabad, and (f) 2008 M_w 7.9 Sichuan earthquakes. Causative fault and off-fault splays are in black, rupture surface trace is in red, zone of largest coseismic surface slips is in green (≥80% of maximum slip, dashed line), and hypocenter (with 5 km uncertainty) as H. Slip mode and overall structural maturity of causative faults are indicated. Rupture speeds are noted in red where available. More details and references on earthquake and fault parameters can be found in Text S1 and Table S1.

profiles in the direction(s) of fault lengthening [*Peacock and Sanderson*, 1991, 1994, 1996; *Nicol et al*., 1996; *Manighetti et al*., 2001a; *Davis et al*., 2005]. Structural maturity is hence variable along a fault. Hereafter, we refer to the local maturity as the "along-strike maturity." It is not possible at present to quantify along-strike maturity by simple metrics, because fault age, net slip, and slip rate data are too scarce along faults. However, it is certain that maturity decreases systematically along a fault from the zone of fault initiation to the current location of the fault propagating tip(s). Hence, knowledge of the fault propagation direction(s) is sufficient to identify the most mature and least mature sections of a fault.

A concrete example is the ~1400 km long North Anatolian fault. The fault initiated in the east ~13 Ma ago [e.g., *Sengör et al*., 1985; *Armijo et al*., 1999; *Bohnhoff et al*., 2016]; it then propagated westward at ~20 cm/yr [*Hubert-Ferrari et al*., 2003] so that its central part formed at ~8.5 Ma [*Hubert-Ferrari et al*., 2002], its western part across the Sea of Marmara at ~5 Ma [*Schindler*, 1998; *Armijo et al*., 1999], and its western propagating tip entered the Aegean Sea ~1 Ma ago [*Armijo et al*., 1996]. Therefore, regarding its overall maturity, we classify the North Anatolian fault as globally mature, and regarding its along-strike maturity, we identify its

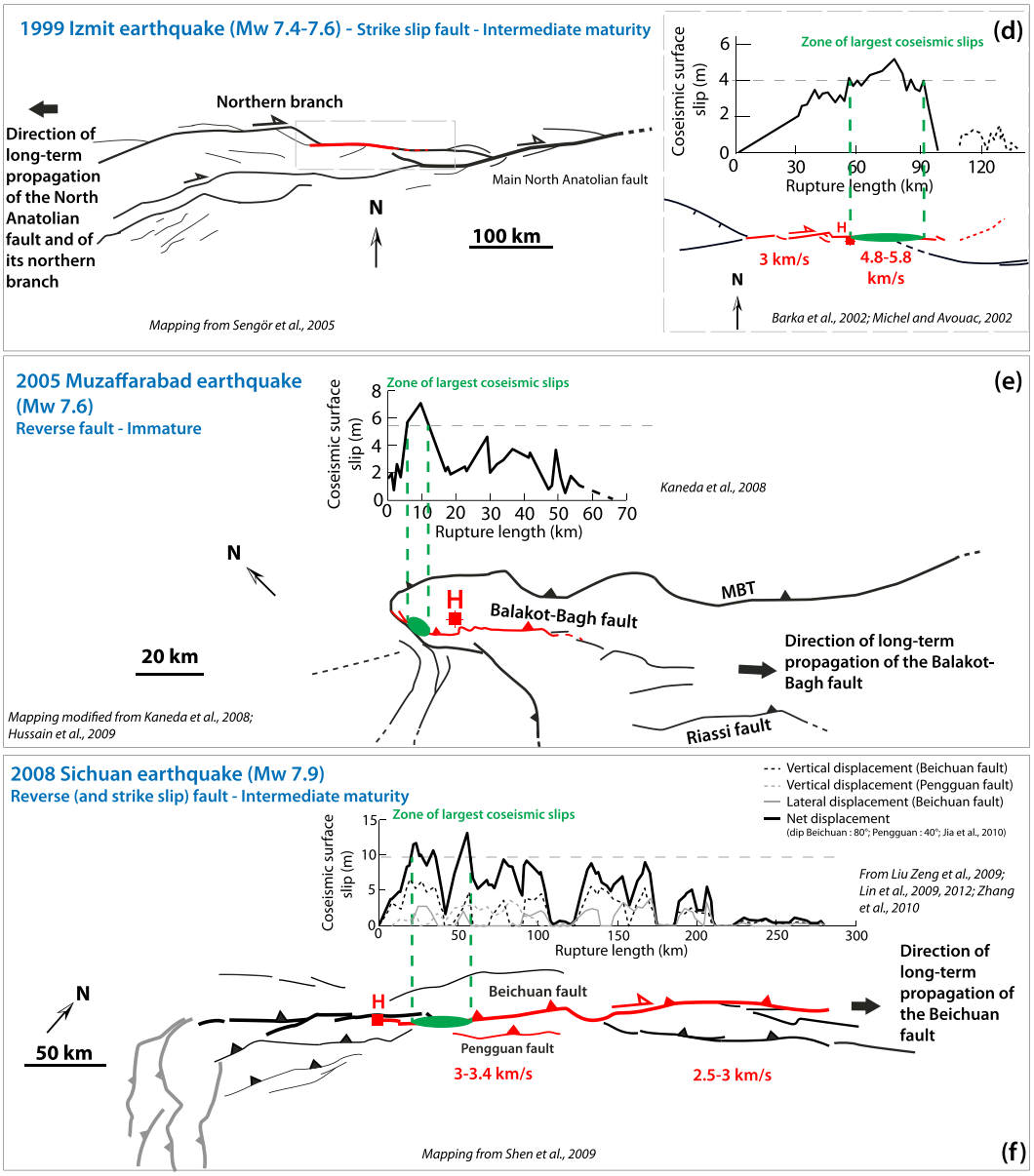

Figure 1. (continued)

easternmost part as the most mature and its westernmost part as the least mature. In this particular example, because constraints on local fault age are available we can even qualify the along-strike maturity in absolute terms: the easternmost section is mature and the westernmost section is immature.

3. Earthquake and Fault Data

Here we summarize the earthquake and fault data we have compiled. A detailed description and complete reference list are provided in Text S1 and Table S1 in the supporting information. Because uncertainties on most fault and earthquake parameters cannot be quantified with simple metrics, we estimate their relative quality, generally on the basis of the number and consistency of available data (Text S1). The relative quality attributes are compiled in Table S2, so as to provide a comprehensive view of the robustness of the data.

The 27 large earthquakes we analyze are instrumental and historical continental events that were well documented in prior studies. They span a broad range of magnitudes (M_w 6.5–8.1), maximum coseismic slips at the surface (0.4–14 m), rupture lengths (25–475 km), slip modes (67% strike slip, 18% normal, and 15% reverse),

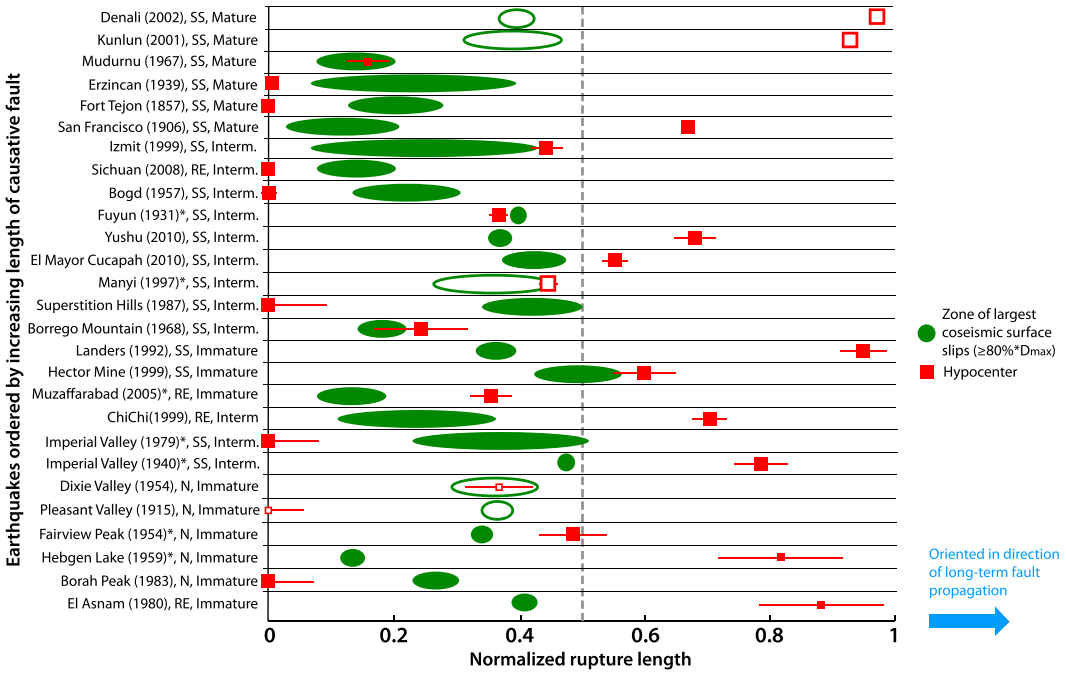

Figure 2. Position of zone of largest surface slip (green) relative to rupture length for 27 earthquakes. Earthquakes are ordered by increasing length of their causative fault. Slip mode and overall structural maturity of causative faults are indicated (SS, strike slip; N, normal; R, reverse). For each earthquake, the rupture has been oriented so that the direction of long-term fault propagation (and hence decreasing fault structural maturity) is on the right side of the figure. If fault propagation is bilateral (empty symbols), we assume that fault growth initiated near the present fault center and consider the half-fault length which hosts most of the rupture. Earthquakes with an asterisk are those for which the direction of long-term propagation of their causative fault is more poorly constrained (quality Q3 in Table S2). Hypocenters (H) are shown with a 5 km uncertainty; poorly constrained hypocenters are represented with a smaller symbol. More details and references on earthquake and fault parameters can be found in Text S1 and Table S1.

locations worldwide, and tectonic settings. Their causative faults have also various ages (1–60 Ma), net slips (from <1 to 600 km), lengths (25–2300 km), and slip rates (0.2–35 mm/yr).

The earthquake and fault parameters we analyze are the following (see Figures 1 and S1):

1. *Maps of surface traces of earthquake ruptures*. Those are available for all the earthquakes we analyze and are generally consistent among studies.
2. *Measured surface slip profiles along entire rupture lengths*. Generally, the various slip profiles available for a given earthquake are consistent, especially on the large-scale features that interest us, such as envelope shape and location of largest slip.
3. *Earthquake slip distributions at depth inferred through finite source inversion*. We used 25 published finite source rupture models available for 13 out of the 27 analyzed earthquakes. From each slip model we derive a subsurface slip profile as in *Manighetti et al.* [2005]: at each position along strike we extract the maximum slip value over all depths. For a given earthquake, the large-scale features of subsurface slip profiles that interest us are generally consistent among available slip models. The models provide additional information (Table S3) on rupture width (~22 km on average for all earthquakes) and depth of largest slip (~6 km on average for all earthquakes).
4. *Earthquake hypocenter locations*. Because uncertainties of hypocenter locations are rarely provided, we have assigned to all epicenter coordinates a conservative uncertainty of 5 km in both horizontal directions.
5. *Rupture speed estimates at multiple locations along the rupture*. These are available for 12 out of the 27 earthquakes (Text S1). From these data, we summarize the rupture speeds on each of the two halves (i.e., most mature versus most immature) of the ruptures (Table S4).
6. *Maps of surface traces of earthquake causative faults*. We generally collected these from tectonic studies different from those where the earthquakes are described. These maps provide different levels of detail. Yet the resolution differences do not alter the analysis of the large-scale features that interest us, including

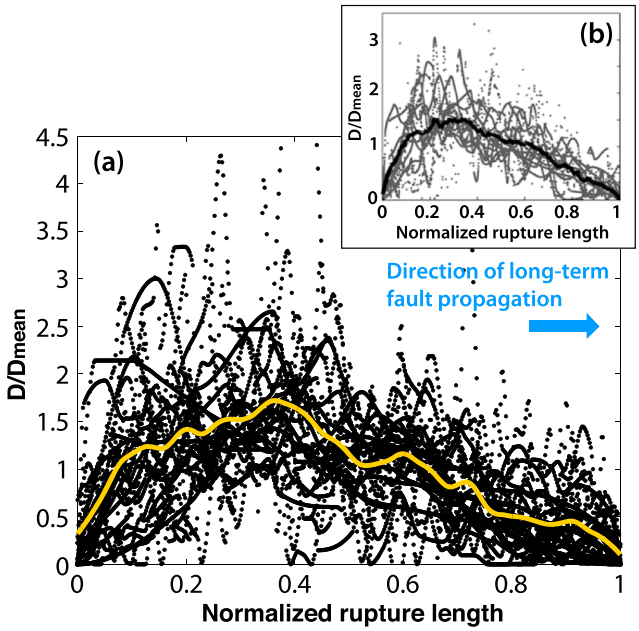

Figure 3. (a) All surface slip profiles normalized by their rupture length and mean slip, oriented so that direction of long-term fault propagation is on the right. Bilateral fault propagation treated as in Figure 2. In yellow is the running average curve for the entire collection of slip profiles. (b) Normalized earthquake surface slip profiles oriented so that the maximum slip appears always on the left, from *Manighetti et al.* [2005]. Details and references on earthquake slip profiles can be found in Text S1 and Table S1.

parent fault length, overall architecture and extent of associated fault networks, and overall location of largest coseismic slips within causative faults. We were able to locate the rupture traces precisely onto the long-term fault maps (see Text S1).

7. *Degree of overall structural maturity of the causative faults*. We have used the classifications of *Manighetti et al.* [2007], as specified in section 2, to classify the overall structural maturity. The population includes 40% of immature faults, 17% of mature faults, and 43% of faults with intermediate overall maturity.
8. *Direction(s) of long-term fault propagation*. All faults studied here have been active over long time spans $\geq$1 Myr, during which they have likely propagated laterally. Indeed, 90% of the faults have a length (L_f) greater than twice the average seismogenic thickness (i.e., $L_f > \sim 40$ km). We derived their direction(s) of long-term propagation from published geological data documenting the along-strike variation in their ages and net slips. Although such data are generally few, they are sufficient to reveal the direction(s) of overall fault age and/or net slip decrease. In some cases, the along-strike decrease of the fault slip rate, the observation that fault segment (s) near the actual fault tip(s) are the youngest or the observation that fault segments become less interconnected in one or two directions along the fault, provide additional or alternative information to derive the direction(s) of long-term fault propagation. The large-scale architecture of the fault zones provides complementary information. All faults have indeed one or both of their tips surrounded by large-scale networks of secondary fault branches, forming a fan of splay faults (see Figures 1 and S1). The presence and geometry of such tip splay networks have been shown to indicate the direction of long-term propagation of the parent faults [*McGrath and Davison*, 1995; *Manighetti et al.*, 1998; *Kim et al.*, 2003; *de Joussineau and Aydin*, 2007; *Faulkner et al.*, 2011; *Perrin et al.*, 2016]. Combining the information above, the directions of long-term propagation are well constrained for ~75% of the faults (Table S2). The San Andreas fault is a particular case: while the Southern San Andreas fault has propagated southward [e.g., *Powell and Weldon*, 1992; *Hull and Nicholson*, 1992; *Sims*, 1993; *Nicholson et al.*, 1994; *Lutz et al.*, 2006; *Kirby et al.*, 2007; *Dorsey et al.*, 2012], the northern San Andreas fault had a more complex history due to its formation in interaction with a subduction zone [e.g., *Atwater*, 1970; *Nicholson et al.*, 1994; *Atwater and Stock*, 1998] (details in Text S1). Therefore, the northern San Andreas fault did not propagate laterally as intraplate faults do. Yet the age and amount of lateral slip vary along its length, decreasing from north to south [e.g., *Nicholson et al.*, 1994; *Atwater and Stock*, 1998; *Liu et al.*, 2010] (see Text S1). Therefore, in the figures that follow, "direction of long-term propagation" should read only as "direction of decreasing maturity" for the special case of the northern San Andreas fault.

4. Distribution of Earthquake Slip and Rupture Speed in Relation to Long-Term Fault Propagation

For each event in Figures 1 and S1, we identify a "zone of largest slip" in which surface slip exceeds 80% of its maximum (shown in green). In all cases, there is a single zone of largest slip on the ruptured fault. Increasing

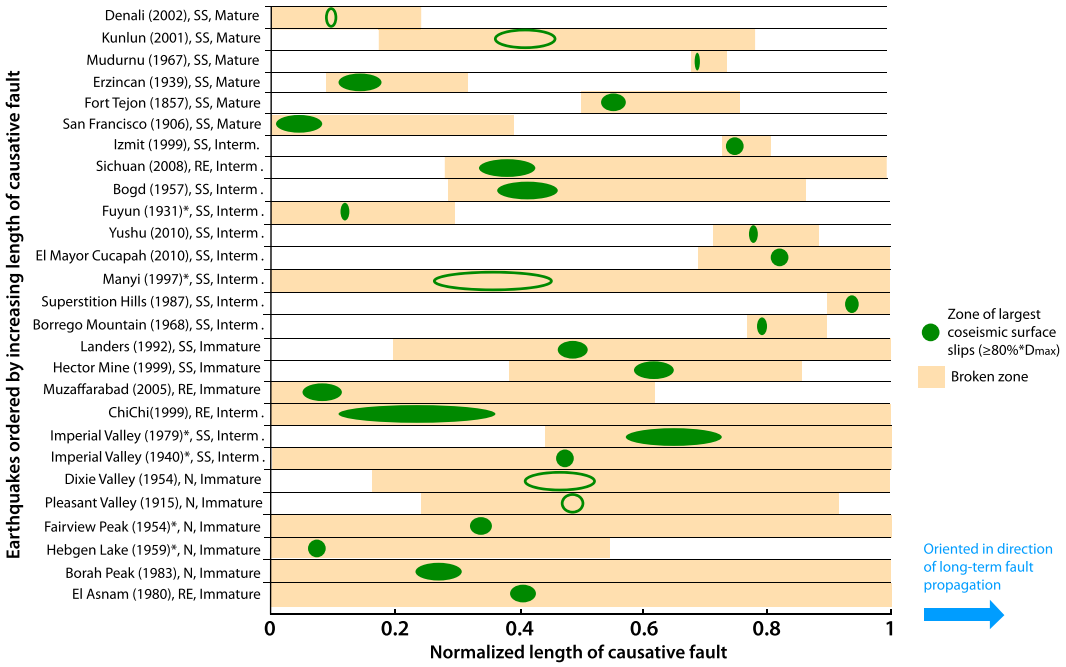

Figure 4. Location of ruptured sections and zones of largest surface slip along entire causative faults. Largest slip defined as in Figure 2. Half-fault length is shown for faults with bilateral propagation. Earthquakes with an asterisk as in Figure 2. On each fault, the rupture zone is in orange, and the white parts are the fault sections left unbroken. Note that the Izmit rupture is here represented with respect to overall North Anatolian fault zone. We observe that some earthquakes broke a mature fault section (e.g., Denali, Erzincan, Hebgen Lake, Fuyun, Muzaffarabad, and San Francisco), others broke an immature fault section (e.g., Borrego Mountain, El Mayor Cucapah, Fort Tejon, Hector Mine, Imperial Valley 1979, Izmit, Mudurnu, Superstition Hills, and Yushu), a few others broke a fault section with intermediate maturity (e.g., Kunlun, Sichuan, and Bogd), and a few others broke or almost broke the entire fault (or half fault in bilateral cases) (e.g., Manyi, Landers, Chi-Chi, Imperial Valley 1940, Dixie Valley, Pleasant Valley, Fairview Peak, Borah Peak, and El Asnam). Independent of these differences, largest coseismic slips systematically locate on most mature portions of rupture zones (i.e., left part of the orange zones).

the fraction of slip taken to represent the largest displacements does not modify the finding of a single, large slip zone (Figure S3). The zones of largest surface slips are generally colocated with those inferred at depth (compare Figures S1 and S2), and therefore, considering slip at depth does not affect our analysis (see Figures S2 and S4).

For all earthquakes, Figure 2 shows the position of the zone of largest slip relative to the rupture length. Each rupture is oriented so that the direction of long-term fault propagation appears on the right side. If long-term fault growth is bilateral, we assume that the fault initiated near its present center, as described in Text S1, and consider only the rupture part hosted on the half-fault length. The fault slip mode and overall maturity are indicated, which allows comparing the results on normal, reverse, and strike-slip faults of different overall maturities. We find that for all earthquakes, the largest coseismic slips are systematically located on the half of the rupture most distant from the long-term fault propagation tip, that is, in the most mature part of the rupture zone. This finding is independent of the earthquake slip mode, magnitude, length, and overall maturity of the causative fault. In contrast, there is no systematic spatial relation between the zone of largest slip and the hypocenter location; they can be close to each other (e.g., Hector Mine, Borrego Mountain, Manyi, and Fuyun) but are more often distant, sometimes at opposite ends of the rupture (e.g., Denali, Kunlun, and Landers). Earthquake ruptures can thus propagate over long distances either toward or away from the zone of largest slip. These observations are similar when slip at depth is considered (Figures S2 and S4).

In Figure 3a, the surface slip profiles have been normalized by their mean value and rupture length (the running average is shown as a yellow curve). As in Figure 2, they have been oriented so that the direction of long-term fault propagation is on the right side. In Figure 3a, all earthquakes are shown together, but we discriminate strike-slip and dip-slip ruptures in Figures S5a and S5b. Both figures confirm that the largest coseismic slips are in the left half of the plot, i.e., in the most mature parts of the rupture zones, regardless of earthquake slip mode, magnitude, length, and overall maturity of the causative fault. In addition, we observe that the coseismic slip systematically tapers over a long distance (on average, 60% of the rupture length) in the

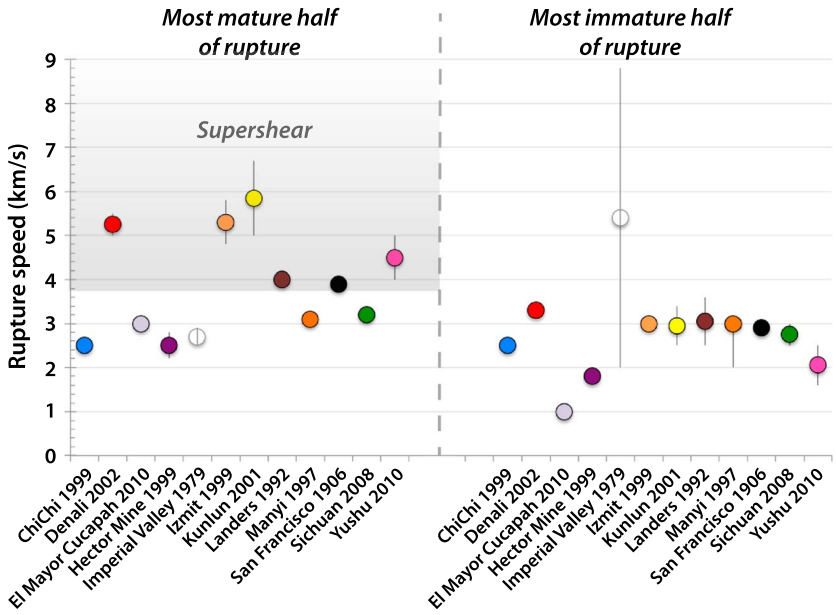

Figure 5. Rupture speeds estimated for 12 of the analyzed earthquakes, along with their uncertainties (data in Table S4). For each earthquake, the rupture speeds along the most mature and along the most immature halves of the ruptures (relative maturity inferred from direction of long-term fault propagation) are plotted with a same color. All ruptures (except for possibly the 1979 Imperial Valley, whose rupture speed is not well constrained) have propagated faster, sometimes with supershear speed, along the most mature part of the ruptures.

direction of long-term fault propagation and hence in the direction of decreasing along-strike maturity. In contrast to a similar figure by *Manighetti et al*. [2005] (reproduced here in Figure 3b), in which the slip profiles were oriented so that the maximum slip appeared on the left, in the present study the maximum slip is systematically located on the left part of Figure 3a not by design but as a natural result of the slip profiles being oriented in the direction of long-term fault propagation.

In Figure 4, we examine the location of zones of largest coseismic slip relative to the entire causative faults. The faults have been oriented as before so that the direction of their long-term propagation is to the right (bilateral cases treated as before). The figure examines the earthquake slip behavior with respect to the relative distance from the propagating fault tip. Most earthquakes did not rupture the entire fault length. Some of the ruptures plot in the left part of the graph and hence broke a relatively mature section of their causative fault, far away from the propagating fault tip (e.g., Denali, Erzincan, San Francisco, and Fuyun); other ruptures rather plot at the right end of the graph and hence broke relatively immature sections of their causative fault close to the propagating fault tip (e.g., Izmit, Yushu, Superstition Hills, El Major Cucapah, and Borrego Mountain). Whether an earthquake broke a more mature or a more immature part of its causative fault, its zone of largest slip is skewed toward the most mature part of the rupture zone. However, the degree of slip asymmetry is higher in ruptures on mature fault sections: the distance between the largest slip location and the (right) least mature rupture end, normalized by rupture length, is 85% in the average slip profile of earthquakes on mature fault sections and 65% for earthquakes on immature sections (see Figures S5c and S5d).

In Figure 5 (data in Table S4), we have reported the available rupture propagation speeds, along with their uncertainties (estimated here as the range of values reported by different studies of a same earthquake, when available), distinguishing those in the most mature half of the rupture from those in its most immature half. While rupture speeds are subshear in the most immature broken fault sections, they are systematically faster in the most mature parts of the rupture zones, up to supershear. An exception is the 1979 Imperial Valley earthquake, but its rupture speed and southern rupture portion are not well constrained. The estimated uncertainties on rupture speed are not large enough to mask the overall trend we highlight.

Commonly, large earthquakes do not rupture the entire length of their causative fault, as seen in Figures S1 and 4. Present knowledge of large earthquake sequences that combined to rupture an entire fault is limited because their duration is generally longer than human observation time. Figure 6 reports,

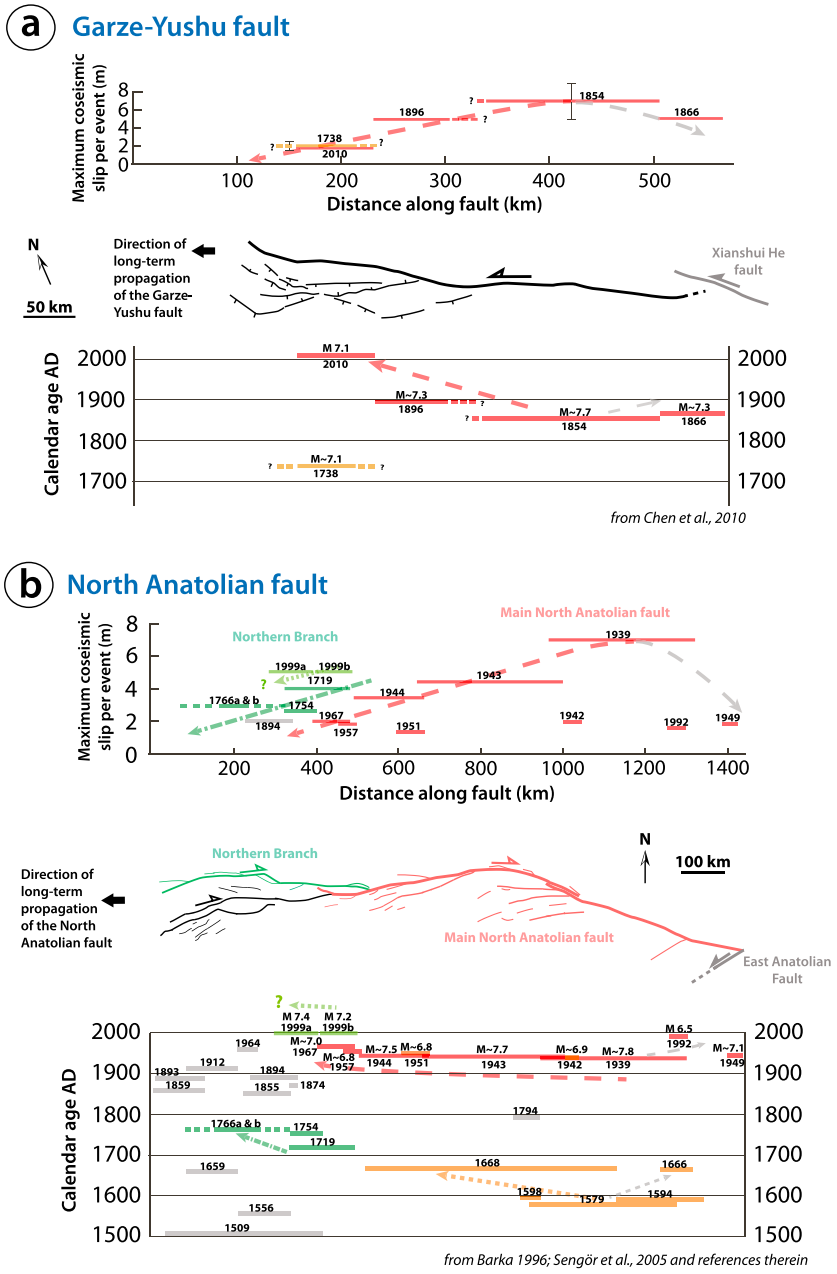

Figure 6. Sequences of large historical earthquakes that combined to rupture a fault entirely. (a) Garze-Yushu fault and (b) North Anatolian fault. In Figures 6a and 6b, long-term fault map is shown in the middle, earthquake time history at the bottom, and maximum surface slips of historical earthquakes at the top. In time plots, arrows suggest earthquake clusters that broke the fault entirely (for North Anatolian, main fault is shown in reddish and Northern Branch in greenish). In slip plots, arrows show slip decrease among clustered events. Slip decreases in the direction of long-term fault propagation.

however, two sequences of large earthquake sequences that are fairly well documented and examines the earthquake slip distribution with respect to the long-term fault propagation. One sequence was a cluster of four large earthquakes which broke entirely the ~450 km long Garze-Yushu fault in ~ 150 years [*Chen et al.*, 2010]. Another sequence comprises eight large earthquakes that broke the main strand of the North Anatolian fault (in red in Figure 6b) in the last century (1939–1967 sequence: *Barka* [1996]; the 1999 Izmit and Duzce earthquakes broke the northern branch of the North Anatolian fault, in green in Figure 6b). In both cases, the slips produced by the largest of these earthquakes were greatest on the most mature section of the fault and decreased progressively in its direction of long-term propagation. The three large earthquakes that ruptured

the northern branch of the North Anatolian fault in the eighteen century (dark greenish colors, Figure 6b) seem to have shown a similar behavior, with largest slips in the eastern, most mature section of the northern branch fault. The Izmit and Duzce earthquakes which occurred later on this northern branch also produced slips consistent with the overall pattern described above. Therefore, sequences of large earthquakes that combine to break a fault entirely seem to produce larger slips in the most mature part of the fault and slips decreasing overall in the direction of long-term fault propagation.

Taken together, the observations above first show that the skewed, semitriangular pattern of earthquake slip distributions (Figure 3) [*Scholz and Lawler*, 2004; *Manighetti et al*., 2005; *Wesnousky*, 2008] is independent of whether the earthquake occurs on a more mature or on a more immature section of the fault. The observations further suggest that the earthquake slip asymmetry is related to the direction of long-term propagation of the causative fault: coseismic slip is systematically largest in the most mature part of the rupture zone and decreases almost linearly over most of the rupture length in the direction of long-term fault propagation and hence of decreasing maturity (Figures 2–4). In contrast, slip decreases abruptly in the opposite direction (Figure 3). Rupture propagation speeds are subshear in the most immature sections of the rupture and faster in the most mature sections, in some cases supershear (Figure 5). In large earthquake sequences, the total earthquake slip distribution is also asymmetric, with largest slip in the most mature part of the fault (Figure 6).

The relations between earthquake slip distributions and long-term fault propagation are found in every earthquake case we analyzed, despite data uncertainties. This suggests that the trends we report are not fortuitous. These relations are found despite the earthquake population spanning a broad range of magnitudes, slip modes, slip amplitudes, and tectonic settings, and despite the causative fault population spanning a broad range of ages, lengths, net slips, slip rates, and hence different degrees of overall structural maturity. These systematics suggest that the relation between earthquake slip asymmetry and lateral fault growth might be generic for continental faults.

5. Discussion

If the macroscopic characteristics of earthquake slip distributions on continental faults are generic, they likely result from a deterministic, systematic control and are not much influenced by case dependent or local factors such as the nature of rocks around the fault, the thickness of the crust, etc. Our observations suggest that the systematic control might relate to an intrinsic property of the causative faults: the systematic lateral change of their structural maturity that arises from their long-term growth. Yet the question remains of which fault property or properties might change along a continental fault as its maturity increases. Below we examine which fault properties might evolve with maturity (section 5.1), and then we discuss how these properties might impact coseismic slip and speed (section 5.2).

5.1. 3-D Fault Architecture and Strength

Three principal, common properties of faults have been documented on natural continental faults and shown to vary with net slip and hence with maturity: off-fault permanent damage, along-strike fault segmentation, and nonplanarity of the fault surface. Their along-strike variation has not or rarely been addressed, however. We present in Figure 7 our conceptual vision of their lateral variations in relation to fault growth, for a continental, crustal, strike-slip fault. The general picture is similar for a dip-slip fault (see Figure S6 in the supporting information) because we are concerned here with properties that mostly relate to the common fault lengthening process.

As they grow, faults damage the embedding crust [e.g., *McGrath and Davison*, 1995; *Cooke*, 1997; *Vermilye and Scholz*, 1998; *Cowie and Shipton*, 1998; *Kim et al*., 2003; *Manighetti et al*., 2004; *Myers and Aydin*, 2004; *de Joussineau et al*., 2007; *de Joussineau and Aydin*, 2007; *Dieterich and Smith*, 2009; *Mitchell and Faulkner*, 2009; *Aydin and Berryman*, 2010; *Savage and Brodsky*, 2011; *Faulkner et al*., 2011] (inset Figure 7). Part of the damage occurs dynamically during earthquakes [e.g., *Schaff and Beroza*, 2004; *Manighetti et al*., 2005; *Andrews*, 2005; *Brenguier et al*., 2008], part of it might be driven by static stress concentration near the tips of the growing fault [e.g., *Lehner et al*., 1981; *Cooke*, 1997; *Willemse and Pollard*, 1998; *Aydin and Berryman*, 2010]. The irreversible part of the damage accumulates to form a wake of microscopic and macroscopic cracks, fractures, and subsidiary faults that altogether constitute a permanent damage zone with altered rock properties and reduced elastic moduli [e.g., *Scholz et al*., 1993; *Chester and Chester*, 1998; *Sibson*, 2003;

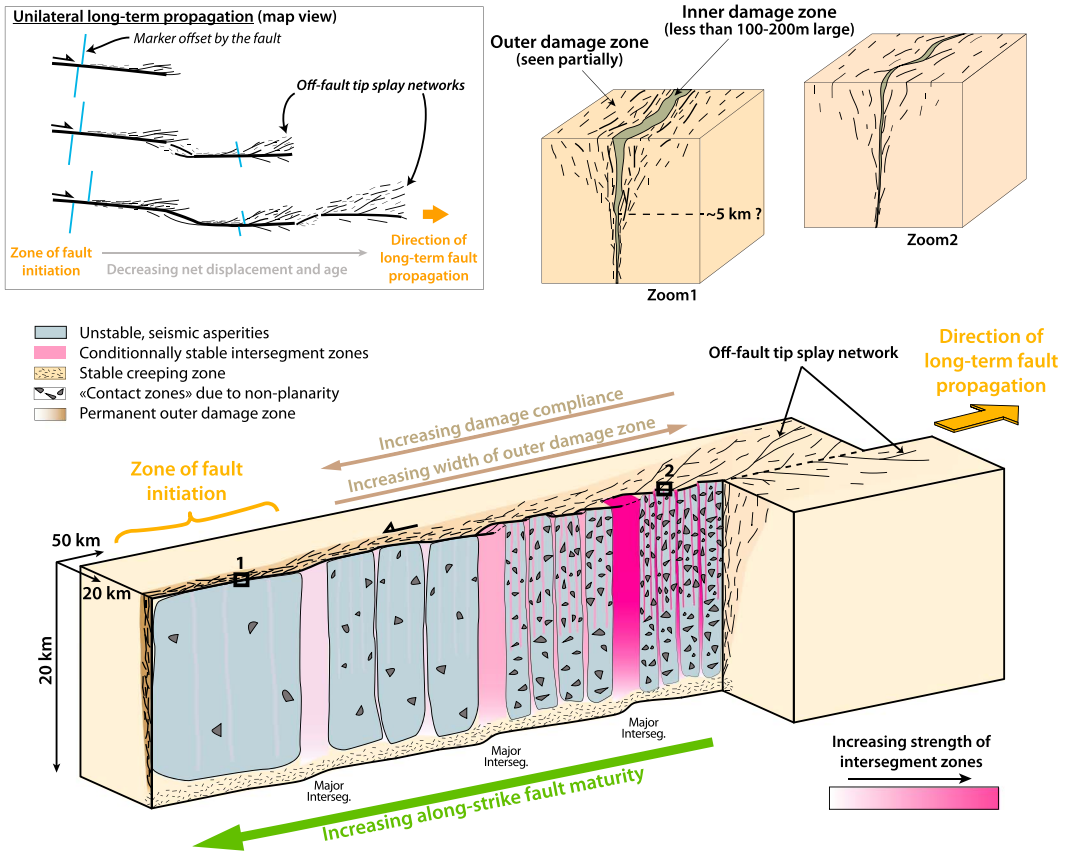

Figure 7. Along-strike evolution of off-fault damage, fault segmentation, and fault planarity with increasing maturity along fault strike. The example fault is strike slip (a dip-slip example is shown in Figure S6). The zone where the fault originally initiated is placed to the left, and it is assumed that the fault lengthened rightward over its lifetime. Fault age, net displacement, and along-strike maturity thus decrease rightward. Inset is a sketch of long-term fault propagation (unilateral case), showing enlargement of the outer damage zone and increased connection of segments in the direction of propagation. The two zooms are close-up views to distinguish the inner and outer damage zones (core is not represented for clarity). The along-strike changes in structural maturity induce changes in off-fault damage width and compliance, fault strength, and fault fracture energy. See text for more discussion.

Manighetti et al., 2004; *Mitchell and Faulkner*, 2009; *Cochran et al.*, 2009; *Aydin and Berryman*, 2010; *Savage and Cooke*, 2010; *Smith et al.*, 2013] (inset Figure 7). These permanent damage zones have a nested hierarchical architecture [e.g., *Sibson*, 1977; *Mitchell and Faulkner*, 2009; *Finzi et al.*, 2009; *Cochran et al.*, 2009; *Shelef and Oskin*, 2010]. The principal slip zone or "fault core" is a few 0.1–1 m thick and includes slip surfaces and highly fractured, disaggregated, and crushed rocks commonly referred to as fault gouge. The core slip zone is surrounded by an "inner damage zone," up to few 100 m wide, where rocks are densely fractured and brecciated (Figure 7 and zooms) [e.g., *Dor et al.*, 2006, 2008; *Mitchell and Faulkner*, 2009; *Sagy and Brodsky*, 2009; *Shelef and Oskin*, 2010; *Faulkner et al.*, 2011; *Savage and Brodsky*, 2011; *Smith et al.*, 2013]. The width of the inner damage zone seems to saturate with fault slip [*Mitchell and Faulkner*, 2009; *Faulkner et al.*, 2011; *Savage and Brodsky*, 2011]. The inner zone is surrounded by a wider "outer damage zone" made of more distributed damage in the form of secondary faults [e.g., *McGrath and Davison*, 1995; *Vermilye and Scholz*, 1999; *Davatzes and Aydin*, 2003; *Manighetti et al.*, 2004; *de Joussineau et al.*, 2007; *de Joussineau and Aydin*, 2007; *Mitchell and Faulkner*, 2009; *Aydin and Berryman*, 2010; *Shelef and Oskin*, 2010; *Faulkner et al.*, 2011; *Perrin et al.*, 2016]. The across-fault width (W_d) of the outer damage zone scales with the parent fault length (L_f) ($W_d \sim 10\%L_f$) [*Perrin et al.*, 2016] and hence increases in the direction of fault lengthening. This results in permanent damage zones that are narrower around the more mature sections of their parent fault and wider around the more immature sections. Seismological studies additionally suggest that while inner damage zones might extend down to the base of the seismogenic crust [e.g., *Evans et al.*, 2000; *Mitchell and Faulkner*, 2009; *Wegler et al.*, 2009; *Viegas et al.*, 2010; *Griffith et al.*, 2012; *Smith et al.*, 2013; *Valoroso et al.*, 2013, 2014; *Liu et al.*, 2014;

Carpenter et al., 2016] (zooms in Figure 7), outer damage zones are more shallow, extending down to ~5 km [*Ben-Zion et al*., 2003; *Peng et al*., 2003; *Lewis et al*., 2005; *Finzi et al*., 2009; *Lewis and Ben-Zion*, 2010; *Yang and Zhu*, 2010; *Yang et al*., 2011; *Allam and Ben-Zion*, 2012; *Allam et al*., 2014; *Zigone et al*., 2015] (zooms in Figure 7).

To our knowledge, there exists no study that estimates damage compliance along a fault as a function of its varying net slip. In Table S5, we have compiled the seismic velocity reductions and compliances that have been measured at different sites along the northern San Andreas, San Jacinto, Elsinore, North Anatolian, Garze-Yushu, and Longmen Shan faults (references in Table S5). These data show that for each fault, damage compliance (damage taken here as a whole) is higher around the most mature parts of the fault and lower around its most immature sections. More generally, larger velocity reductions and lower rigidities are measured around mature faults such as the San Andreas fault (50–60% of rigidity reduction, see *Jolivet et al*. [2009]; 35–50% of velocity reduction, see *McGuire and Ben-Zion* [2005]), whereas smaller velocity reductions are found around more immature faults such as the Garze-Yushu and Longmen Shan faults (velocity reduction $<$ ~8% and ~10%, respectively, see *Yang et al*. [2015] and *Lei and Zhao* [2009]). Therefore, although the question is still begging for more data, available estimates suggest that damage compliance is greater around the most mature parts of the faults.

Another fundamental property of faults is their along-strike segmentation. Faults are divided along their length into discrete subparallel segments of different sizes separated by geometrical discontinuities, generally step overs, called "intersegments" [e.g., *Segall and Pollard*, 1980; *Sibson*, 1986; *Barka and Kadinsky-Cade*, 1988; *Aydin and Schultz*, 1990; *Peacock*, 1991; *Walsh et al*., 2003; *Manighetti et al*., 2009, 2015; *De Joussineau and Aydin*, 2009; *Dieterich and Richards-Dinger*, 2010; *Giba et al*., 2012]. At least the largest intersegments, which separate the longest fault segments, are of crustal scale [e.g., *Sibson*, 1986; *Allam and Ben-Zion*, 2012; *Valoroso et al*., 2014; *Allam et al*., 2014]. *Manighetti et al*. [2009, 2015] and *Otsuki and Dilov* [2005] showed that fault segmentation follows a generic hierarchical structure at its largest scales: regardless of their length, faults contain a similar number of largest-scale segments (i.e., longest segments within a fault), each one in turn containing a similar number of subordinate segments (two to four segments). Data available on the faults we analyzed confirm that 87% of these faults are divided into two to four major segments (Table S1), consistent with general observations. Therefore, the generic segmentation of faults produces a remarkable, deterministic horizontal division of their plane (Figure 7).

Intersegments are regions of distributed and pervasive cracking and faulting [e.g., *King*, 1983; *Manighetti et al*., 2004; *De Joussineau and Aydin*, 2009; *Allam and Ben-Zion*, 2012; *Allam et al*., 2014] (inset Figure 7) that accommodate off-fault deformation at the expense of on-fault slip [e.g., *Dawers and Anders*, 1995; *Manighetti et al*., 2001a; *Davis et al*., 2005]. However, natural fault data show that as a fault accumulates more displacement, its discrete segments increasingly coalesce so as to form a throughgoing fault, whereas on-fault slip deficit at the intersegments is smoothed off [e.g., *Wesnousky*, 1988; *Peacock*, 1991; *Stirling et al*., 1996; *Rahe et al*., 1998; *Walsh et al*., 1999; *Ferrill et al*., 1999; *Manighetti et al*., 2001a, 2009, 2015; *Soliva and Benedicto*, 2004; *Cembrano et al*., 2005; *De Joussineau and Aydin*, 2009; *Aydin and Berryman*, 2010; *Marliyani et al*., 2013] (Figure 7). This is commonly described as the accumulation of slip leading to a geometrically simpler fault [e.g., *Wesnousky*, 1988; *Ben-Zion and Sammis*, 2003; *King and Wesnousky*, 2007; *Wechsler et al*., 2010]. The evolution of on-fault slip at intersegments shows that immature intersegments, where on-fault slip deficit is pronounced, are zones of high fault strength which likely act as mechanical barriers to earthquake slip (e.g., *Scholz and Lawler* [2004], *Dieterich and Richards-Dinger* [2010], and *Allam et al*. [2014]; for a theoretical definition of earthquake barriers, see *Das and Aki* [1977], *Nur* [1978], and *Boatwright and Cocco* [1996]), whereas more mature intersegments, where on-fault slip deficit is reduced, have a lower strength. Therefore, segmentation also produces a lateral heterogeneity in the fault strength. Resistant intersegments of different sizes punctuate the most immature parts of a fault, while their density and strength decrease progressively in the direction of greater maturity. If we call "seismic asperity" a fault segment of roughly homogeneous strength, the length of seismic asperities increases in the direction of increasing maturity (Figure 7).

Finally, fault planes are rough surfaces. The nature of fault roughness is not completely understood, one reason being that fault roughness cannot be observed at the relevant seismogenic depth. Fault roughness has thus only been described so far from limited exposures of fault scarps formed at shallow depth and from surface rupture traces [*Renard et al*., 2006; *Candela et al*., 2009, 2011, 2012; *Brodsky et al*., 2011]. Based on these observations, it has generally been suggested that increasing slip reduces the fault roughness [*Cooke*, 1997; *Choy and Kirby*, 2004; *Sagy et al*., 2007; *Sagy and Brodsky*, 2009; *Mitchell and Faulkner*, 2009; *Wechsler et al*.,

2010; *Savage and Brodsky*, 2011]. We argue that fault segmentation significantly contributes to the nonplanarity of fault surfaces because, whatever their length, fault segments are separated across strike or connected through fault bends. Although continued slip tends to smooth off the smallest step overs and bends, especially along strike-slip faults [e.g., *Nur*, 1978; *Stirling et al*., 1996; *Choy and Kirby*, 2004; *Newman and Ashley Griffith*, 2014], some remain on the fault plane even after segments have coalesced [*Klinger*, 2010; *Candela et al*., 2012]. We suggest that these small-scale nonplanar features form small "contact zones" or "protrusions" on the fault plane and hence produce roughness (Figure 7). We anticipate that the density of such protrusions decreases in the direction of net slip increase. Therefore, the most mature seismic asperities, which host fewer contacts and are smoother, have a smaller fracture energy than the rest of the fault (less contact zones needing to be broken) [e.g., *Tinti et al*., 2005; *Ben-David et al*., 2010]. They are thus zones that are most prone to be broken efficiently [e.g., *Cooke and Murphy*, 2004; *Tinti et al*., 2005; *Fang and Dunham*, 2013; *Newman and Ashley Griffith*, 2014].

In the framework of fault structural evolution presented here, the observations we reported in section 4 suggest that largest coseismic slips and faster rupture speeds are systematically produced (i) on fault sections embedded in narrowest but most compliant damage zones, (ii) on more mature fault segments and therefore on longer seismic asperities with more homogeneous strength, and (iii) on smoother fault sections with lower fracture energy.

5.2. Relations Between 3-D Fault Architecture and Strength, and Earthquake Slip and Speed

We found that earthquake slip asymmetry is independent of the location of earthquake initiation relative to the rupture. Therefore, the slip asymmetry is not or not significantly controlled by dynamic effects that depend on rupture direction. This observation is difficult to explain in the framework of bimaterial interface rupture models which predict rupture propagation preferentially in the direction of motion of the more compliant side of the fault [e.g., *Ben-Zion and Huang*, 2002; *Brietzke and Ben-Zion*, 2006; *Shi and Ben-Zion*, 2006]. In particular, pulse-like rupture models on bimaterial faults generate slip asymmetry [*Ampuero and Ben-Zion*, 2008] but generally in association with a preference for rupture and slip asymmetry in the direction of displacement of the most compliant material. This is not what is observed here since all earthquake cases show slip asymmetry, regardless of their rupture direction.

Therefore, we rather propose that the systematic location of largest coseismic slips in the most mature part of a rupture zone is primarily a static effect, resulting from the elastostatic relation between stress drop, slip, and elastic modulus of the faulted medium. In linear elasticity, earthquake slip roughly equals stress drop multiplied by a characteristic rupture length and divided by the elastic shear modulus of the faulted medium. In a fault surrounded by damaged material, the elastic modulus is expected to decrease as a function of decreasing distance to the fault [e.g., *Huang and Ampuero*, 2011], and an effective shear modulus is approximately given by the harmonic average of the local modulus over an off-fault distance comparable to the rupture length [see *Kaneko et al*., 2011, equation E2]. Hence, even if stress drop is constant over the rupture, the strong reduction of elastic modulus in the zone of most intense damage—at least the inner damage zone—leads to significantly larger slip. For the ruptures analyzed here, the zones of largest coseismic slips are located at an average depth of ~6 km, where the inner and even possibly the outer damage zones exist.

The rationale we propose is consistent with the simulations by *Cappa et al*. [2014] of ruptures embedded in an existing damage zone whose compliance increases and width decreases in one direction along the fault. In these models a constant stress drop rupture develops an asymmetric slip profile with the largest slip in the most compliant part of the rupture. The effect of greater compliance is not offset by the narrower width of the mature damage zone. The earthquake stress drops need not depend on the overall fault maturity. In their empirical study of earthquake slip-to-length ratios versus overall fault structural maturity, *Manighetti et al*. [2007] reached a similar conclusion since they showed that stress drops range between ~3 and 7 MPa (estimated from surface earthquake data) and hence are fairly constant, whatever the degree of overall structural maturity of the broken faults. The lower stress drop values were found, however, on the most mature faults.

Therefore, a constant stress drop well reproduces the observation of earthquake slip asymmetry. This suggests that variations in on-fault prestresses and dynamic friction do not play a significant role in the generic earthquake slip distributions. This further supports the suggestion that bimaterial effects have a limited role on the earthquake slip distribution.

The distribution of fault strength is also expected to contribute to the earthquake slip asymmetry. Prior works have suggested on a theoretical basis that earthquake slip distributions might be controlled by strength and stress variations along fault planes [e.g., *Das and Aki*, 1977; *Nur*, 1978; *Israel and Nur*, 1979; *Madariaga*, 1979; *Bürgmann et al*., 1994; *Boatwright and Cocco*, 1996; *Cooke*, 1997; *Noda and Lapusta*, 2010; *Kaneko et al*., 2010]. The reduction of on-fault slip deficit at intersegments in the direction of greater maturity leads to longer fault segments in that direction (see *Bohnhoff et al*. [2016] for related observations on the North Anatolian fault). As shown by *Madariaga* [1979], the seismic moment of a multisegment rupture is controlled by the length of the broken segments. Hence, slip is expected to be larger on portions of the fault that have longer segments because of their greater maturity.

The faster rupture speeds found along the most mature parts of the ruptures (Figure 5) suggest that earthquake dynamics is influenced by the along-strike changes of fault maturity. This observation is consistent with dynamic rupture simulations showing an enhancement of rupture speed and supershear transition on faults surrounded by damaged zones [*Huang et al*., 2014, 2016]. Preexisting damage reduces the rupture speed of subshear ruptures by a moderate amount (several 10%). This reduction is comparable to uncertainties in rupture speed estimates; hence, it is difficult to robustly observe this effect of damage on subshear ruptures. Our observations instead relate to the effect of damage on supershear ruptures, which is stronger. Dynamic rupture models in homogeneous media show that a rupture becomes supershear beyond some critical propagation distance, if the initial stress exceeds a critical threshold [*Andrews*, 1976; *Dunham*, 2007]. The presence of a low-velocity damage zone reduces both the critical distance and the stress threshold: the more compliant the damage zone, the shorter the critical distance and the smaller the stress threshold [*Huang et al*., 2016]. Therefore, a rupture in a more damaged zone has a higher chance to jump to supershear speeds. While seismological support for this mechanism was found in a few earthquakes [*Huang et al*., 2016], our study provides evidence from a broad set of large earthquakes.

Systematic along-strike variations of fault strength controlled by maturity can also contribute to rupture speed patterns. We suggest that two earthquake situations might occur. Some earthquakes are observed to nucleate at the edge of a mature zone (e.g., Bogd, Borah Peak, Borrego Mountain, Dixie Valley, El Mayor Cucapah, Erzincan, Fairview Peak, Fort Tejon, Fuyun, Hector Mine, Imperial Valley 1979, Izmit, Manyi, Mudurnu, Muzzafarbad, Sichuan, and Superstition Hills earthquakes; Figures 2 and S1) and break first a mature, large-slip fault segment, which then triggers the rupture of adjacent more immature fault sections. Observations show that the rupture speed in the primary, mature rupture zone is fast, up to supershear. Other earthquakes nucleate in more immature fault sections (e.g., Chi-Chi, Denali, El Asnam, Hebgen Lake, Imperial Valley 1940, Kunlun, Landers, San Francisco, and Yushu earthquakes; Figures 2 and S1) then propagate in the direction of greater maturity. As they propagate, they encounter less resistance in larger and smoother seismic asperities (i.e., barriers are fewer or easier to skip, and seismic asperities have smaller fracture energy due to fewer contacts; Figure 7; see also *Das* [2007] for similar finding) and they gather higher driving energy from larger slip promoted by increasing off-fault compliance. Altogether, these factors likely contribute to accelerate the rupture in the direction of greater maturity.

These factors also make rupture arrest less and less likely as the rupture progresses in the direction of increasing maturity, yet ruptures stop systematically at the very edge of the zone that hosts the largest slips. We infer that rupture arrest is governed by an additional factor, namely an "external barrier" which can be either a strong "tectonic feature" (e.g., a very strong intersegment, an intersection with an oblique fault) or a major stress gap resulting from a prior earthquake release or from insufficient stress loading [e.g., *Husseini et al*., 1975; *Nur*, 1978; *Scholz*, 1998; *Scholz and Lawler*, 2004]. Whatever the reason, slip profiles suggest that the rupture arrest is abrupt and hence prone to generate strong ground motions [*Madariaga*, 1983].

6. Conclusions

Our analysis of 27 large ($M_w \geq 6.5$) continental earthquakes and their causative faults shows that the largest slips and higher rupture speeds are most likely to occur on the half of the rupture most distant from the long-term fault propagation tips, that is, in the most mature half of the ruptured fault section. Our empirical observations, with support from dynamic rupture models, suggest that asymmetry of earthquake slip and rupture speed in large continental earthquakes is likely governed by along-strike heterogeneity of (i) material compliance and strength off the fault as a result of permanent damage, (ii) strength on the fault as a result of

lateral fault segmentation, and (iii) fault fracture energy as a result of fault roughness. We suggest that these heterogeneities along faults are systematic because they result from the long-term fault growth process. Our results thus provide important insight on the connection between long-term fault evolution and rupture dynamics processes. They validate earlier suggestions that seismic characteristics of a fault evolve in tandem with its structural evolution [*Wesnousky*, 1988; *Wechsler et al*., 2010].

Our results might have important practical implications for earthquake hazard mitigation. The direction(s) in which a fault has been propagating over its lifetime can be determined from geological evidence. Based on this prior tectonic knowledge, it seems possible to anticipate on which side of the fault future earthquake slips and rupture speeds will tend to be larger. Moreover, once earthquake initiation is identified on a continental fault whose long-term propagation direction is known, it seems possible to anticipate in which direction earthquake slip may increase and rupture may accelerate. This information can be constrained in real time and could critically contribute to earthquake early warning systems, helping anticipate sites of largest ground motions and warn populations on the way of the growing rupture [e.g., *Böse and Heaton*, 2010; *Böse et al*., 2012, 2015].

Acknowledgments
The data used in this paper are available in the literature. We are grateful to three anonymous reviewers and to the Editor Y. Ben-Zion for their constructive, thorough comments that greatly helped us in improving our manuscript.

References

Allam, A. A., and Y. Ben-Zion (2012), Seismic velocity structures in the Southern California plate-boundary environment from double-difference tomography, *Geophys. J. Int.*, *190*(2), 1181–1196.
Allam, A. A., Y. Ben-Zion, I. Kurzon, and F. Vernon (2014), Seismic velocity structure in the Hot Springs and Trifurcation areas of the San Jacinto Fault Zone, California, from double-difference tomography, *Geophys. J. Int.*, *198*(2), 978–999.
Ampuero, J.-P., and Y. Ben-Zion (2008), Cracks, pulses and macroscopic asymmetry of dynamic rupture on a bimaterial interface with velocity-weakening friction, *Geophys. J. Int.*, *173*(2), 674–692, doi:10.1111/j.1365-246X.2008.03736.x.
Anderson, J. G., S. G. Wesnousky, and M. W. Stirling (1996), Earthquake size as a function of fault slip rate, *Bull. Seismol. Soc. Am.*, *86*(3), 683–690.
Andrews, D. J. (1976), Rupture velocity of plane strain shear cracks, *J. Geophys. Res.*, *81*(32), 5679–5687, doi:10.1029/JB081i032p05679.
Andrews, D. J. (2005), Rupture dynamics with energy loss outside the slip zone, *J. Geophys. Res.*, *110*, B01307, doi:10.1029/2004JB003191.
Armijo, R., B. G. C. P. Meyer, G. C. P. King, A. Rigo, and D. Papanastassiou (1996), Quaternary evolution of the Corinth Rift and its implications for the late Cenozoic evolution of the Aegean, *Geophys. J. Int.*, *126*(1), 11–53.
Armijo, R., B. Meyer, A. Hubert, and A. Barka (1999), Westward propagation of the North Anatolian fault into the northern Aegean: Timing and kinematics, *Geology*, *27*, 267–270, doi:10.1130/0091-7613.
Atwater, T. (1970), Implications of plate tectonics for the Cenozoic tectonic evolution of western North America, *Geol. Soc. Am. Bull.*, *81*, 3513–3536, doi:10.1130/0016-7606(1970)81[3513:IOPTFT]2.0.CO;2.
Atwater, T., and J. Stock (1998), Pacific-North America plate tectonics of the Neogene southwestern United States: An update, *Int. Geol. Rev.*, *40*(5), 375–402.
Aydin, A., and J. G. Berryman (2010), Analysis of the growth of strike-slip faults using effective medium theory, *J. Struct. Geol.*, *32*(11), 1629–1642.
Aydin, A., and R. A. Schultz (1990), Effect of mechanical interaction on the development of strike-slip faults with echelon patterns, *J. Struct. Geol.*, *12*(1), 123–129.
Barka, A. (1996), Slip distribution along the North Anatolian fault associated with the large earthquakes of the period 1939 to 1967, *Bull. Seismol. Soc. Am.*, *86*(5), 1238–1254.
Barka, A., et al. (2002), The surface rupture and slip distribution of the 17 August 1999 Izmit earthquake (*M* 7.4), North Anatolian fault, *Bull. Seismol. Soc. Am.*, *92*(1), 43–60.
Barka, A. A., and K. Kadinsky-Cade (1988), Strike-slip fault geometry in Turkey and its influence on earthquake activity, *Tectonics*, *7*(3), 663–684, doi:10.1029/TC007i003p00663.
Ben-David, O., S. M. Rubinstein, and J. Fineberg (2010), Slip-stick and the evolution of frictional strength, *Nature*, *463*(7277), 76–79.
Bennett, E., J. Youngson, J. Jackson, R. Norris, G. Raisbeck, and F. Yiou (2006), Combining geomorphic observations with in situ cosmogenic isotope measurements to study anticline growth and fault propagation in Central Otago, New Zealand, *N. Z. J. Geol. Geophys.*, *49*(2), 217–231.
Bennett, E. R., J. H. Youngson, J. A. Jackson, R. J. Norris, G. M. Raisbeck, F. Yiou, and E. Fielding (2005), Growth of South Rough Ridge, Central Otago, New Zealand: Using in situ cosmogenic isotopes and geomorphology to study an active, blind reverse fault, *J. Geophys. Res.*, *110*, B02404, doi:10.1029/2004JB003184.
Ben-Zion, Y., and Y. Huang (2002), Dynamic rupture on an interface between a compliant fault zone layer and a stiffer surrounding solid, *J. Geophys. Res.*, *107*(B2), 2042, doi:10.1029/2001JB000254.
Ben-Zion, Y., and C. G. Sammis (2003), Characterization of fault zones, *Pure Appl. Geophys.*, *160*(3-4), 677–715.
Ben-Zion, Y., et al. (2003), A shallow fault-zone structure illuminated by trapped waves in the Karadere–Duzce branch of the North Anatolian Fault, western Turkey, *Geophys. J. Int.*, *152*(3), 699–717.
Boatwright, J., and M. Cocco (1996), Frictional constraints on crustal faulting, *J. Geophys. Res.*, *101*, 13,895–13,909, doi:10.1029/96JB00405.
Bohnhoff, M., P. Martínez-Garzón, F. Bulut, E. Stierle, and Y. Ben-Zion (2016), Maximum earthquake magnitudes along different sections of the North Anatolian fault zone, *Tectonophysics*, *674*, 147–165.
Böse, M., and T. H. Heaton (2010), Probabilistic prediction of rupture length, slip and seismic ground motions for an ongoing rupture: Implications for early warning for large earthquakes, *Geophys. J. Int.*, *183*, 1014–1030, doi:10.1111/j.1365-246X.2010.04774.x.
Böse, M., T. H. Heaton, and E. Hauksson (2012), Real-time finite fault rupture detector (FinDer) for large earthquakes, *Geophys. J. Int*, *191*(2), 803–812.
Böse, M., C. Felizardo, and T. H. Heaton (2015), Finite-fault rupture detector (FinDer): Going real-time in Californian ShakeAlert Warning System, *Seismol. Res. Lett.*, *86*, 1692–1704.

Bouchon, M. (1997), The state of stress on some faults of the San Andreas system as inferred from near-field strong motion data, *J. Geophys. Res.*, *102*(B6), 11,731–11,744, doi:10.1029/97JB00623.
Brenguier, F., M. Campillo, C. Hadziioannou, N. M. Shapiro, R. M. Nadeau, and E. Larose (2008), Postseismic relaxation along the San Andreas fault at Parkfield from continuous seismological observations, *Science*, *321*(5895), 1478–1481.
Brietzke, G. B., and Y. Ben-Zion (2006), Examining tendencies of in-plane rupture to migrate to material interfaces, *Geophys. J. Int.*, *167*(2), 807–819.
Brodsky, E. E., J. J. Gilchrist, A. Sagy, and C. Collettini (2011), Faults smooth gradually as a function of slip, *Earth Planet. Sci. Lett.*, *302*(1), 185–193.
Bull, J. M., P. M. Barnes, G. Lamarche, D. J. Sanderson, P. A. Cowie, S. K. Taylor, and J. K. Dix (2006), High-resolution record of displacement accumulation on an active normal fault: Implications for models of slip accumulation during repeated earthquakes, *J. Struct. Geol.*, *28*(7), 1146–1166.
Burbank, D., A. Meigs, and N. Brozović (1996), Interactions of growing folds and coeval depositional systems, *Basin Res.*, *8*(3), 199–223.
Bürgmann, R., D. D. Pollard, and S. J. Martel (1994), Slip distributions on faults: Effects of stress gradients, inelastic deformation, heterogeneous host-rock stiffness, and fault interaction, *J. Struct. Geol.*, *16*, 1675–1690, doi:10.1016/0191-8141(94)90134-1.
Candela, T., F. Renard, M. Bouchon, A. Brouste, D. Marsan, J. Schmittbuhl, and C. Voisin (2009), Characterization of fault roughness at various scales: Implications of three-dimensional high resolution topography measurements, *Pure Appl. Geophys.*, *166*(10-11), 1817–1851.
Candela, T., F. Renard, M. Bouchon, J. Schmittbuhl, and E. E. Brodsky (2011), Stress drop during earthquakes: Effect of fault roughness scaling, *Bull. Seismol. Soc. Am.*, *101*(5), 2369–2387.
Candela, T., F. Renard, Y. Klinger, K. Mair, J. Schmittbuhl, and E. E. Brodsky (2012), Roughness of fault surfaces over nine decades of length scales, *J. Geophys. Res.*, *117*, B08409, doi:10.1029/2011JB009041.
Cao, T., and K. Aki (1986), Seismicity simulation with a rate-and state-dependent friction law, *Pure Appl. Geophys.*, *124*(3), 487–513.
Cappa, F., C. Perrin, I. Manighetti, and E. Delor (2014), Off-fault long-term damage: A condition to account for generic, triangular earthquake slip profiles, *Geochem. Geophys. Geosyst.*, *15*, 1476–1493, doi:10.1002/2013GC005182.
Carpenter, B. M., M. J. Ikari, and C. Marone (2016), Laboratory observations of time-dependent frictional strengthening and stress relaxation in natural and synthetic fault gouges, *J. Geophys. Res. Solid Earth*, *121*, 1183–1201, doi:10.1002/2015JB012136.
Cartwright, J. A., B. D. Trudgill, and C. S. Mansfield (1995), Fault growth by segment linkage: An explanation for scatter in maximum displacement and trace length data from the Canyonlands Grabens of SE Utah, *J. Struct. Geol.*, *17*(9), 1319–1326.
Cembrano, J., G. González, G. Arancibia, I. Ahumada, V. Olivares, and V. Herrera (2005), Fault zone development and strain partitioning in an extensional strike-slip duplex: A case study from the Mesozoic Atacama fault system, Northern Chile, *Tectonophysics*, *400*(1), 105–125.
Chen, J., R. Heermance, D. W. Burbank, K. M. Scharer, J. Miao, and C. Wang (2007), Quantification of growth and lateral propagation of the Kashi anticline, southwest Chinese Tian Shan, *J. Geophys. Res.*, *112*, B03S16, doi:10.1029/2006JB004345.
Chen, L., H. Wang, Y. Ran, X. Sun, G. Su, J. Wang, X. B. Tan, Z. M. Li, and X. Zhang (2010), The M_S7. 1 Yushu earthquake surface rupture and large historical earthquakes on the Garzê-Yushu Fault, *Chin. Sci. Bull.*, *55*(31), 3504–3509.
Chester, F. M., and J. S. Chester (1998), Ultracataclasite structure and friction processes of the Punchbowl fault, San Andreas system, California, *Tectonophysics*, *295*(1), 199–221.
Childs, C., A. Nicol, J. J. Walsh, and J. Watterson (2003), The growth and propagation of synsedimentary faults, *J. Struct. Geol.*, *25*, 633–648, doi:10.1016/S0191-8141(02)00054-8.
Choi, J.-H., K. Jin, D. Enkhbayar, B. Davvasambuu, A. Bayasgalan, and Y.-S. Kim (2012), Rupture propagation inferred from damage patterns, slip distribution, and segmentation of the 1957 M_w 8.1 Gobi-Altay earthquake rupture along the Bogd fault, Mongolia, *J. Geophys. Res.*, *117*, B12401, doi:10.1029/2011JB008676.
Choy, G. L., and S. H. Kirby (2004), Apparent stress, fault maturity and seismic hazard for normal-fault earthquakes at subduction zones, *Geophys. J. Int.*, *159*, 991–1012, doi:10.1111/j.1365-246X.2004.02449.x.
Choy, G. L., A. McGarr, S. H. Kirby, and J. Boatwright (2006), An overview of the global variability in radiated energy and apparent stress, in *Earthquakes: Radiated Energy and the Physics of Faulting*, *Geophys. Monogr. Ser.*, edited by R. Abercrombie et al., pp. 43–58, AGU, Washington, D. C.
Cochran, E. S., Y. G. Li, P. M. Shearer, S. Barbot, Y. Fialko, and J. E. Vidale (2009), Seismic and geodetic evidence for extensive, long-lived fault damage zones, *Geology*, *37*, 315–318, doi:10.1130/G25306A.1.
Cooke, M. L. (1997), Fracture localization along faults with spatially varying friction, *J. Geophys. Res.*, *102*, 22,425–22,434, doi:10.1029/97JB01829.
Cooke, M. L., and S. Murphy (2004), Assessing the work budget and efficiency of fault systems using mechanical models, *J. Geophys. Res.*, *109*, B10408, doi:10.1029/2004JB002968.
Cowie, P. A., and C. H. Scholz (1992a), Displacement-length scaling relationship for faults: Data synthesis and discussion, *J. Struct. Geol.*, *14*(10), 1149–1156.
Cowie, P. A., and C. H. Scholz (1992b), Physical explanation for the displacement-length relationship of faults using a post-yield fracture mechanics model, *J. Struct. Geol.*, *14*, 1133–1148, doi:10.1016/0191-8141(92)90065-5.
Cowie, P. A., and Z. K. Shipton (1998), Fault tip displacement gradients and process zone dimensions, *J. Struct. Geol.*, *20*(8), 983–997.
Crone, A. J., and K. M. Haller (1991), Segmentation of basin and range normal faults: Examples from east-central Idaho and southwestern Montana, *J. Struct. Geol.*, *13*, 151–164.
Crone, A. J., and M. N. Machette (1984), Surface faulting accompanying the Borah Peak earthquake, central Idaho, *Geology*, *12*, 664–667.
Crone, A. J., M. N. Machette, M. G. Bonilla, J. J. Lienkaemper, K. L. Pierce, W. E. Scott, and R. C. Bucknam (1987), Surface faulting accompanying the Borah Peak earthquake and segmentation of the Lost River fault, central Idaho, *Bull. Seismol. Soc. Am.*, *77*, 730–770.
D'Alessio, M. A., and S. J. Martel (2004), Fault terminations and barriers to fault growth, *J. Struct. Geol.*, *26*(10), 1885–1896.
Das, S. (2007), The need to study speed, *Science*, *317*(5840), 905–906.
Das, S., and K. Aki (1977), Fault plane with barriers: A versatile earthquake model, *J. Geophys. Res.*, *82*, 5658–5670, doi:10.1029/JB082i036p05658.
Davatzes, N. C., and A. Aydin (2003), The formation of conjugate normal fault systems in folded sandstone by sequential jointing and shearing, Waterpocket monocline, Utah, *J. Geophys. Res.*, *108*(B10), 2478, doi:10.1029/2002JB002289.
Davis, K., D. W. Burbank, D. Fisher, S. Wallace, and D. Nobes (2005), Thrust-fault growth and segment linkage in the active Ostler fault zone, New Zealand, *J. Struct. Geol.*, *27*, 1528–1546, doi:10.1016/j.jsg.2005.04.011.
Dawers, N. H., and M. H. Anders (1995), Displacement-length scaling and fault linkage, *J. Struct. Geol.*, *17*, 607–614, doi:10.1016/0191-8141(94)00091-D.
Dawers, N. H., M. H. Anders, and C. H. Scholz (1993), Growth of normal faults: Displacement-length scaling, *Geology*, *21*(12), 1107–1110.
De Joussineau, G., and A. Aydin (2007), The evolution of the damage zone with fault growth in sandstone and its multiscale characteristics, *J. Geophys. Res.*, *112*, B12401, doi:10.1029/2006JB004711.

De Joussineau, G., and A. Aydin (2009), Segmentation along strike-slip faults revisited, *Pure Appl. Geophys.*, *166*, 1575–1594, doi:10.1007/s00024-009-0511-4.
De Joussineau, G., O. Mutlu, A. Aydin, and D. D. Pollard (2007), Characterization of strike-slip fault–splay relationships in sandstone, *J. Struct. Geol.*, *29*(11), 1831–1842.
Dieterich, J. H., and K. B. Richards-Dinger (2010), Earthquake recurrence in simulated fault systems, in *Seismogenesis and Earthquake Forecasting: The Frank Evison*, vol. 2, pp. 233–250, Springer, Basel.
Dieterich, J. H., and D. E. Smith (2009), Nonplanar faults: Mechanics of slip and off-fault damage, *Pure Appl. Geophys.*, *166*, 1799–1815.
Dolan, J. F., and B. D. Haravitch (2014), How well do surface slip measurements track slip at depth in large strike-slip earthquakes? The importance of fault structural maturity in controlling on-fault slip versus off-fault surface deformation, *Earth Planet. Sci. Lett.*, *388*, 38–47.
Dor, O., T. K. Rockwell, and Y. Ben-Zion (2006), Geological observations of damage asymmetry in the structure of the San Jacinto, San Andreas and Punchbowl faults in Southern California: A possible indicator for preferred rupture propagation direction, *Pure Appl. Geophys.*, *163*, 301–349, doi:10.1007/s00024-005-0023-9.
Dor, O., C. Yildirim, T. K. Rockwell, Y. Ben-Zion, O. Emre, M. Sisk, and T. Y. Duman (2008), Geological and geomorphologic asymmetry across the rupture zones of the 1943 and 1944 earthquakes on the North Anatolian Fault: Possible signals for preferred earthquake propagation direction, *Geophys. J. Int.*, *173*(2), 483–504.
Dorsey, R. J., G. J. Axen, T. C. Peryam, and M. E. Kairouz (2012), Initiation of the southern Elsinore fault at ~1.2 Ma: Evidence from the Fish Creek–Vallecito Basin, southern California, *Tectonics*, *31*(2), TC2006, doi:10.1029/2011TC003009.
Du, Y., and A. Aydin (1995), Shear fracture patterns and connectivity at geometric complexities along strike-slip faults, *J. Geophys. Res.*, *100*(B9), 18,093–18,102, doi:10.1029/95JB01574.
Dunham, E. M. (2007), Conditions governing the occurrence of supershear ruptures under slip-weakening friction, *J. Geophys. Res.*, *112*, B07302, doi:10.1029/2006JB004717.
Evans, J. P., Z. Shipton, M. A. Pachell, S. Lim, and K. Robeson (2000), The structure and composition of exhumed faults, and their implications for seismic processes, in *Proceedings of the 3rd Conference on Tectonic Problems of the San Andreas Fault System*, pp. 67–81, Stanford Univ, Calif.
Fang, Z., and E. M. Dunham (2013), Additional shear resistance from fault roughness and stress levels on geometrically complex faults, *J. Geophys. Res. Solid Earth*, *118*, 3642–3654, doi:10.1002/jgrb.50262.
Faulkner, D. R., T. M. Mitchell, E. Jensen, and J. Cembrano (2011), Scaling of fault damage zones with displacement and the implications for fault growth processes, *J. Geophys. Res.*, *116*, B05403, doi:10.1029/2010JB007788.
Ferrill, D. A., J. A. Stamatakos, and D. Sims (1999), Normal fault corrugation: Implications for growth and seismicity of active normal faults, *J. Struct. Geol.*, *21*(8), 1027–1038.
Finzi, Y., E. H. Hearn, Y. Ben-Zion, and V. Lyakhovsky (2009), Structural properties and deformation patterns of evolving strike-slip faults: Numerical simulations incorporating damage rheology, *Pure Appl. Geophys.*, *166*(10-11), 1537–1573.
Giba, M., J. J. Walsh, and A. Nicol (2012), Segmentation and growth of an obliquely reactivated normal fault, *J. Struct. Geol.*, *39*, 253–267.
Griffith, W. A., T. M. Mitchell, J. Renner, and G. Di Toro (2012), Coseismic damage and softening of fault rocks at seismogenic depths, *Earth Planet. Sci. Lett.*, *353*, 219–230.
Hecker, S., T. E. Dawson, and D. P. Schwartz (2010), Normal-faulting slip maxima and stress-drop variability: A geological perspective, *Bull. Seismol. Soc. Am.*, *100*(6), 3130–3147.
Huang, Y., and J. P. Ampuero (2011), Pulse-like ruptures induced by low-velocity fault zones, *J. Geophys. Res.*, *116*, B12307, doi:10.1029/2011JB008684.
Huang, Y., J.-P. Ampuero, and D. V. Helmberger (2014), Earthquake ruptures modulated by waves in damaged fault zones, *J. Geophys. Res. Solid Earth*, *119*, 3133–3154, doi:10.1002/2013JB010724.
Huang, Y., J.-P. Ampuero, and D. V. Helmberger (2016), The potential for supershear earthquakes in damaged fault zones—Theory and observations, *Earth Planet. Sci. Lett.*, *433*, 109–115, doi:10.1016/j.epsl.2015.10.046.
Hubert-Ferrari, A., R. Armijo, G. King, B. Meyer, and A. Barka (2002), Morphology, displacement, and slip rates along the North Anatolian Fault, Turkey, *J. Geophys. Res.*, *107*(B10), 2235, doi:10.1029/2001JB000393.
Hubert-Ferrari, A., G. King, I. Manighetti, R. Armijo, B. Meyer, and P. Tapponnier (2003), Long-term elasticity in the continental lithosphere; modelling the Aden Ridge propagation and the Anatolian extrusion process, *Geophys. J. Int.*, *153*, 111–132, doi:10.1046/j.1365-246X.2003.01872.x.
Hull, A. G., and C. Nicholson (1992), Seismotectonics of the northern Elsinore fault zone, southern California, *Bull. Seismol. Soc. Am.*, *82*, 800–818.
Hussain, A., R. S. Yeats, and MonaLisa (2009), Geological setting of the 8 October 2005 Kashmir earthquake, *J. Seismol.*, *13*(3), 315–325.
Husseini, M. I., D. B. Jovanovich, M. J. Randall, and L. B. Freund (1975), The fracture energy of earthquakes, *Geophys. J. Int.*, *43*(2), 367–385.
Ikari, M. J., C. Marone, and D. M. Saffer (2011), On the relation between fault strength and frictional stability, *Geology*, *39*(1), 83–86.
Israel, M., and A. Nur (1979), A complete solution of a one-dimensional propagating fault with nonuniform stress and strength, *J. Geophys. Res.*, *84*, 2223–2234, doi:10.1029/JB084iB05p02223.
Jackson, J., R. Norris, and J. Youngson (1996), The structural evolution of active fault and fold systems in central Otago, New Zealand: Evidence revealed by drainage patterns, *J. Struct. Geol.*, *18*(2), 217–234.
Jackson, J., J. F. Ritz, L. Siame, G. Raisbeck, F. Yiou, R. Norris, J. Youngson, and E. Bennett (2002), Fault growth and landscape development rates in Otago, New Zealand, using in situ cosmogenic 10 Be, *Earth Planet. Sci. Lett.*, *195*(3), 185–193.
Jolivet, R., R. Bürgmann, and N. Houlié (2009), Geodetic exploration of the elastic properties across and within the northern San Andreas Fault zone, *Earth Planet. Sci. Lett.*, *288*(1), 126–131.
Kaneda, H., et al. (2008), Surface rupture of the 2005 Kashmir, Pakistan, earthquake and its active tectonic implications, *Bull. Seismol. Soc. Am.*, *98*(2), 521–557.
Kaneko, Y., J.-P. Avouac, and N. Lapusta (2010), Towards inferring earthquake patterns from geodetic observations of interseismic coupling, *Nat. Geosci.*, *3*, 363–369, doi:10.1038/ngeo843.
Kaneko, Y., J. P. Ampuero, and N. Lapusta (2011), Spectral-element simulations of long-term fault slip: Effect of low-rigidity layers on earthquake-cycle dynamics, *J. Geophys. Res.*, *116*, B10313, doi:10.1029/2011JB008395.
Keller, E. A., R. L. Zepeda, T. K. Rockwell, T. L. Ku, and W. S. Dinklage (1998), Active tectonics at Wheeler Ridge, southern San Joaquin Valley, California, *Geol. Soc. Am. Bull.*, *110*(3), 298–310.
Keller, E. A., L. Gurrola, and T. E. Tierney (1999), Geomorphic criteria to determine direction of lateral propagation of reverse faulting and folding, *Geology*, *27*(6), 515–518.
Kim, Y. S., D. C. P. Peacock, and D. J. Sanderson (2003), Mesoscale strike-slip faults and damage zones at Marsalforn, Gozo Island, Malta, *J. Struct. Geol.*, *25*(5), 793–812.
King, G. (1983), The accommodation of large strains in the upper lithosphere of the Earth and other solids by self-similar fault systems: The geometrical origin of b-Value, *Pure Appl. Geophys.*, *121*, 761–815, doi:10.1007/BF02590182.

King, G. C., and S. G. Wesnousky (2007), Scaling of fault parameters for continental strike-slip earthquakes, *Bull. Seismol. Soc. Am.*, *97*(6), 1833–1840.
Kirby, S. M., S. U. Janecke, R. J. Dorsey, B. A. Housen, V. E. Langenheim, K. A. McDougall, and A. N. Steely (2007), Pleistocene Brawley and Ocotillo formations: Evidence for initial strike-slip deformation along the San Felipe and San Jacinto fault zones, southern California, *J. Geol.*, *115*(1), 43–62.
Klinger, Y. (2010), Relation between continental strike-slip earthquake segmentation and thickness of the crust, *J. Geophys. Res.*, *115*, B07306, doi:10.1029/2009JB006550.
Lavallée, D., P. Liu, and R. J. Archuleta (2006), Stochastic model of heterogeneity in earthquake slip spatial distributions, *Geophys. J. Int.*, *165*(2), 622–640.
Lehner, F. K., V. C. Li, and J. R. Rice (1981), Stress diffusion along rupturing plate boundaries, *J. Geophys. Res.*, *86*(B7), 6155–6169, doi:10.1029/JB086iB07p06155.
Lei, J., and D. Zhao (2009), Structural heterogeneity of the Longmenshan fault zone and the mechanism of the 2008 Wenchuan earthquake (M_s 8.0), *Geochem. Geophys. Geosyst.*, *10*, Q10010, doi:10.1029/2009GC002590.
Lewis, M. A., and Y. Ben-Zion (2010), Diversity of fault zone damage and trapping structures in the Parkfield section of the San Andreas Fault from comprehensive analysis of near fault seismograms, *Geophys. J. Int.*, *183*(3), 1579–1595.
Lewis, M. A., Z. Peng, Y. Ben-Zion, and F. L. Vernon (2005), Shallow seismic trapping structure in the San Jacinto fault zone near Anza, California, *Geophys. J. Int.*, *162*(3), 867–881.
Lin, A., G. Rao, and B. Yan (2012), Field evidence of rupture of the Qingchuan Fault during the 2008 M_w7.9 Wenchuan earthquake, northeastern segment of the Longmen Shan Thrust Belt, China, *Tectonophysics*, *522–523*, 243–252, doi:10.1016/j.tecto.2011.12.012.
Lin, A. M., Z. K. Ren, D. Jia, and X. J. Wu (2009), Co-seismic thrusting rupture and slip distribution produced by the 2008 M_w 7.9 Wenchuan earthquake, China, *Tectonophysics*, *471*, 203–215.
Liu, M., H. Wang, and Q. Li (2010), Inception of the eastern California shear zone and evolution of the Pacific-North American plate boundary: From kinematics to geodynamics, *J. Geophys. Res.*, *115*, B07401, doi:10.1029/2009JB007055.
Liu, Z., J. Huang, Z. Peng, and J. Su (2014), Seismic velocity changes in the epicentral region of the 2008 Wenchuan earthquake measured from three-component ambient noise correlation techniques, *Geophys. Res. Lett.*, *41*, 37–42, doi:10.1002/2013GL058682.
Liu-Zeng, J., T. Heaton, and C. DiCaprio (2005), The effect of slip variability on earthquake slip-length scaling, *Geophys. J. Int.*, *162*(3), 841–849.
Liu-Zeng, J., et al. (2009), Co-seismic ruptures of the 12 May, 2008, M_s 8.0 Wenchuan earthquake, Sichuan: East-west crustal shortening on oblique, parallel thrusts along the eastern edge of Tibet, *Earth Planet. Sc. Lett.*, *286*, 355–370.
Lutz, A. T., R. J. Dorsey, B. A. Housen, and S. U. Janecke (2006), Stratigraphic record of Pleistocene faulting and basin evolution in the Borrego Badlands, San Jacinto fault zone, Southern California, *Geol. Soc. Am. Bull.*, *118*(11-12), 1377–1397.
Madariaga, R. (1979), On the relation between seismic moment and stress drop in the presence of stress and strength heterogeneity, *J. Geophys. Res.*, *84*, 2243–2250, doi:10.1029/JB084iB05p02243.
Madariaga, R. (1983), High frequency radiation from dynamic earthquake fault models, *Ann. Geophys.*, *1*, 17–23.
Mai, P. M., and G. C. Beroza (2002), A spatial random field model to characterize complexity in earthquake slip, *J. Geophys. Res.*, *107*(B11), 2308, doi:10.1029/2001JB000588.
Malagnini, L., S. Nielsen, K. Mayeda, and E. Boschi (2010), Energy radiation from intermediate- to large-magnitude earthquakes: Implications for dynamic fault weakening, *J. Geophys. Res.*, *115*, B06319, doi:10.1029/2009JB006786.
Manighetti, I., P. Tapponnier, V. Courtillot, S. Gruszow, and P. Y. Gillot (1997), Propagation of rifting along the Arabia-Somalia plate boundary: The gulfs of Aden and Tadjoura, *J. Geophys. Res.*, *102*(B2), 2681–2710, doi:10.1029/96JB01185.
Manighetti, I., P. Tapponnier, P. Y. Gillot, E. Jacques, V. Courtillot, R. Armijo, J. C. Ruegg, and G. King (1998), Propagation of rifting along the Arabia-Somalia plate boundary: Into Afar, *J. Geophys. Res.*, *103*(B3), 4947–4974, doi:10.1029/97JB02758.
Manighetti, I., G. C. P. King, Y. Gaudemer, C. H. Scholz, and C. Doubre (2001a), Slip accumulation and lateral propagation of active normal faults in Afar, *J. Geophys. Res.*, *106*, 13,667–13,696, doi:10.1029/2000JB900471.
Manighetti, I., P. Tapponnier, V. Courtillot, Y. Gallet, E. Jacques, and P. Y. Gillot (2001b), Strain transfer between disconnected, propagating rifts in Afar, *J. Geophys. Res.*, *106*(B7), 13,613–13,665, doi:10.1029/2000JB900454.
Manighetti, I., G. King, and C. G. Sammis (2004), The role of off-fault damage in the evolution of normal faults, *Earth Planet. Sci. Lett.*, *217*, 399–408, doi:10.1016/S0012-821X(03)00601-0.
Manighetti, I., M. Campillo, C. Sammis, P. M. Mai, and G. King (2005), Evidence for self-similar, triangular slip distributions on earthquakes: Implications for earthquake and fault mechanics, *J. Geophys. Res.*, *110*, B05302, doi:10.1029/2004JB003174.
Manighetti, I., M. Campillo, S. Bouley, and F. Cotton (2007), Earthquake scaling, fault segmentation, and structural maturity, *Earth Planet. Sci. Lett.*, *253*, 429–438, doi:10.1016/j.epsl.2006.11.004.
Manighetti, I., D. Zigone, M. Campillo, and F. Cotton (2009), Self-similarity of the largest-scale segmentation of the faults: Implications for earthquake behavior, *Earth Planet. Sci. Lett.*, *288*, 370–381, doi:10.1016/j.epsl.2009.09.040.
Manighetti, I., C. Caulet, D. De Barros, C. Perrin, F. Cappa, and Y. Gaudemer (2015), Generic along-strike segmentation of Afar normal faults, East Africa: Implications on fault growth and stress heterogeneity on seismogenic fault planes, *Geochem. Geophys. Geosyst.*, *16*, 443–467, doi:10.1002/2014GC005691.
Mansfield, C., and J. Cartwright (2001), Fault growth by linkage: Observations and implications from analogue models, *J. Struct. Geol.*, *23*, 745–763, doi:10.1016/S0191-8141(00)00134-6.
Marliyani, G. I., T. K. Rockwell, N. W. Onderdonk, and S. F. McGill (2013), Straightening of the Northern San Jacinto Fault, California, as seen in the fault-structure evolution of the San Jacinto Valley Stepover, *Bull. Seismol. Soc. Am.*, *103*(3), 2047–2061.
Marrett, R., and R. W. Allmendinger (1990), Kinematic analysis of fault-slip data, *J. Struct. Geol.*, *12*(8), 973–986.
Martel, S. J. (1997), Effects of cohesive zones on small faults and implications for secondary fracturing and fault trace geometry, *J. Struct. Geol.*, *19*(6), 835–847.
McGrath, A. G., and I. Davison (1995), Damage zone geometry around fault tips, *J. Struct. Geol.*, *17*(7), 1011–1024.
McGuire, J., and Y. Ben-Zion (2005), High-resolution imaging of the Bear Valley section of the San Andreas Fault at seismogenic depths with fault-zone head waves and relocated seismicity, *Geophys. J. Int.*, *163*(1), 152–164.
Meyer, B., P. Tapponnier, L. Bourjot, Y. Metivier, G. Gaudemer, G. Peltzer, G. Shunmin, and C. Zhitai (1998), Crustal thickening in Gansu–Qinghai, lithospheric mantle subduction, and oblique, strike–slip controlled growth of the Tibetan plateau, *Geophys. J. Int.*, *135*, 1–48.
Michel, R., and J. P. Avouac (2002), Deformation due to the 17 August 1999 Izmit, Turkey, earthquake measured from SPOT images, *J. Geophys. Res.*, *107*(B4), 2062, doi:10.1029/2000JB000102.
Mitchell, T. M., and D. R. Faulkner (2009), The nature and origin of off-fault damage surrounding strike-slip fault zones with a wide range of displacements: A field study from the Atacama fault system, northern Chile, *J. Struct. Geol.*, *31*(8), 802–816.
Moore, D. E., and D. A. Lockner (1995), The role of microcracking in shear-fracture propagation in granite, *J. Struct. Geol.*, *17*(1), 95–114.

Morewood, N. C., and G. P. Roberts (1999), Lateral propagation of the surface trace of the South Alkyonides normal fault segment, central Greece: Its impact on models of fault growth and displacement–length relationships, *J. Struct. Geol.*, *21*(6), 635–652.
Mueller, K., and P. Talling (1997), Geomorphic evidence for tear faults accommodating lateral propagation of an active fault-bend fold, Wheeler Ridge, California, *J. Struct. Geol.*, *19*(3), 397–411.
Mutlu, O., and D. D. Pollard (2008), On the patterns of wing cracks along an outcrop scale flaw: A numerical modeling approach using complementarity, *J. Geophys. Res.*, *113*, B06403, doi:10.1029/2007JB005284.
Myers, R., and A. Aydin (2004), The evolution of faults formed by shearing across joint zones in sandstone, *J. Struct. Geol.*, *26*(5), 947–966.
Newman, P. J., and W. Ashley Griffith (2014), The work budget of rough faults, *Tectonophysics*, *636*, 100–110, doi:10.1016/j.tecto.2014.08.007.
Nicholson, C., C. C. Sorlien, T. Atwater, J. C. Crowell, and B. P. Luyendyk (1994), Microplate capture, rotation of the western Transverse Ranges, and initiation of the San Andreas transform as a low-angle fault system, *Geology*, *22*(6), 491–495.
Nicol, A., J. Watterson, J. J. Walsh, and C. Childs (1996), The shapes, major axis orientations and displacement patterns of fault surfaces, *J. Struct. Geol.*, *18*(2), 235–248.
Nicol, A., J. Walsh, K. Berryman, and S. Nodder (2005), Growth of a normal fault by the accumulation of slip over millions of years, *J. Struct. Geol.*, *27*(2), 327–342.
Nicol, A., J. J. Walsh, P. Villamor, H. Seebeck, and K. R. Berryman (2010), Normal fault interactions, paleoearthquakes and growth in an active rift, *J. Struct. Geol.*, *32*(8), 1101–1113.
Niemeijer, A., C. Marone, and D. Elsworth (2010), Frictional strength and strain weakening in simulated fault gouge: Competition between geometrical weakening and chemical strengthening, *J. Geophys. Res.*, *115*, B10207, doi:10.1029/2009JB000838.
Noda, H., and N. Lapusta (2010), Three-dimensional earthquake sequence simulations with evolving temperature and pore pressure due to shear heating: Effect of heterogeneous hydraulic diffusivity, *J. Geophys. Res.*, *115*, B12314, doi:10.1029/2010JB007780.
Nur, A. (1978), Nonuniform friction as a physical basis for earthquake mechanics, in *Rock Friction and Earthquake Prediction*, pp. 964–989, Birkhäuser Basel, Basel, doi:10.1007/978-3-0348-7182-2_26.
Otsuki, K., and T. Dilov (2005), Evolution of hierarchical self-similar geometry of experimental fault zones: Implications for seismic nucleation and earthquake size, *J. Geophys. Res.*, *110*, B03303, doi:10.1029/2004JB003359.
Peacock, D. C. P. (1991), Displacements and segment linkage in strike-slip fault zones, *J. Struct. Geol.*, *13*(9), 1025–1035.
Peacock, D. C. P., and D. J. Sanderson (1991), Displacements, segment linkage and relay ramps in normal fault zones, *J. Struct. Geol.*, *13*(6), 721–733.
Peacock, D. C. P., and D. J. Sanderson (1994), Geometry and development of relay ramps in normal fault systems, *AAPG Bull.*, *78*(2), 147–165.
Peacock, D. C. P., and D. J. Sanderson (1996), Effects of propagation rate on displacement variations along faults, *J. Struct. Geol.*, *18*(2), 311–320.
Peng, Z., Y. Ben-Zion, A. J. Michael, and L. Zhu (2003), Quantitative analysis of seismic fault zone waves in the rupture zone of the 1992 Landers, California, earthquake: Evidence for a shallow trapping structure, *Geophys. J. Int.*, *155*(3), 1021–1041.
Perrin, C., I. Manighetti, and Y. Gaudemer (2016), Off-fault tip splay networks: A genetic and generic property of faults indicative of their long-term propagation, *C. R. Geosci.*, *348*, 52–60, doi:10.1016/j.crte.2015.05.002.
Powell, R. E., and R. J. Weldon II (1992), Evolution of the San Andreas fault, *Annu. Rev. Earth Planet. Sci.*, *20*, 431–468, doi:10.1146/annurev.ea.20.050192.002243.
Radiguet, M., F. Cotton, I. Manighetti, M. Campillo, and J. Douglas (2009), Dependency of near-field ground motions on the structural maturity of the ruptured faults, *Bull. Seismol. Soc. Am.*, *99*(4), 2572–2581.
Rahe, B., D. A. Ferrill, and A. P. Morris (1998), Physical analog modeling of pull-apart basin evolution, *Tectonophysics*, *285*(1), 21–40.
Renard, F., C. Voisin, D. Marsan, and J. Schmittbuhl (2006), High resolution 3D laser scanner measurements of a strike-slip fault quantify its morphological anisotropy at all scales, *Geophys. Res. Lett.*, *33*, L04305, doi:10.1029/2005GL025038.
Sagy, A., and E. E. Brodsky (2009), Geometric and rheological asperities in an exposed fault zone, *J. Geophys. Res.*, *114*, B02301, doi:10.1029/2008JB005701.
Sagy, A., E. E. Brodsky, and G. J. Axen (2007), Evolution of fault-surface roughness with slip, *Geology*, *35*(3), 283–286.
Savage, H. M., and E. E. Brodsky (2011), Collateral damage: Evolution with displacement of fracture distribution and secondary fault strands in fault damage zones, *J. Geophys. Res.*, *116*, B03405, doi:10.1029/2010JB007665.
Savage, H. M., and M. L. Cooke (2010), Unlocking the effects of friction on fault damage zones, *J. Struct. Geol.*, *32*(11), 1732–1741.
Schaff, D. P., and G. C. Beroza (2004), Coseismic and postseismic velocity changes measured by repeating earthquakes, *J. Geophys. Res.*, *109*, B10302, doi:10.1029/2004JB003011.
Schindler, C. (1998), Geology of NW Turkey: Results of the Marmara polyproject, in *Active Tectonics of Northwestern Anatolia: The Marmara Poly-Project, a Multidisciplinary Approach by Space-Geodesy, Geology, Hydrology, Geothermics and Seismology*, pp. 329–375, Verlag de Fachvereine, Zurich.
Schlagenhauf, A., I. Manighetti, J. Malavieille, and S. Dominguez (2008), Incremental growth of normal faults: Insights from a laser-equipped analog experiment, *Earth Planet. Sci. Lett.*, *273*(3), 299–311.
Schlische, R. W., S. S. Young, R. V. Ackermann, and A. Gupta (1996), Geometry and scaling relations of a population of very small rift-related normal faults, *Geology*, *24*(8), 683–686.
Scholz, C. H. (1998), Earthquakes and friction laws, *Nature*, *391*, 37–42, doi:10.1038/34097.
Scholz, C. H. (2006), The strength of the San Andreas Fault: A critical analysis, in *Earthquakes: Radiated Energy and the Physics of Faulting*, *Geophys. Monogr. Ser.*, vol. 170, pp. 301–311, AGU, Washington, D. C.
Scholz, C. H., and T. M. Lawler (2004), Slip tapers at the tips of faults and earthquake ruptures, *Geophys. Res. Lett.*, *31*, L21609, doi:10.1029/2004GL021030.
Scholz, C. H., N. H. Dawers, J. Z. Yu, M. H. Anders, and P. A. Cowie (1993), Fault growth and fault scaling laws: Preliminary results, *J. Geophys. Res.*, *98*(B12), 21,951–21,961, doi:10.1029/93JB01008.
Segall, P., and D. D. Pollard (1980), Mechanics of discontinuous faults, *J. Geophys. Res.*, *85*, 4337–4350, doi:10.1029/JB085iB08p04337.
Segall, P., and D. D. Pollard (1983), Nucleation and growth of strike slip faults in granite, *J. Geophys. Res.*, *88*, 555–568, doi:10.1029/JB088iB01p00555.
Sengör, A. M. C., N. Görür, and F. Saroglu (1985), Strike-slip faulting and related basin formation in zones of tectonic escape: Turkey as a case study, in *Strike-Slip Faulting and Basin Formation*, edited by K. T. Biddle and N. Christie-Blick, *Soc. Econ. Paleontol. Mineral. Spec. Publ.*, *37*, 227–264, doi:10.2110/pec.85.37.0227.
Shelef, E., and M. Oskin (2010), Deformation processes adjacent to active faults: Examples from eastern California, *J. Geophys. Res.*, *115*, B05308, doi:10.1029/2009JB006289.
Shen, Z. K., J. B. Sun, P. Z. Zhang, Y. G. Wan, M. Wang, R. Bürgmann, Y. Zeng, W. Gan, H. Liao, and Q. Wang (2009), Slip maxima at fault junctions and rupturing of barriers during the 2008 Wenchuan earthquake, *Nat. Geosci.*, *2*, 718–724.

Shi, Z., and Y. Ben-Zion (2006), Dynamic rupture on a bimaterial interface governed by slip-weakening friction, *Geophys. J. Int.*, *165*(2), 469–484.
Sibson, R. H. (1977), Fault rocks and fault mechanisms, *J. Geol. Soc.*, *133*(3), 191–213.
Sibson, R. H. (1986), Rupture interaction with fault jogs, *Earthquake Source Mech.*, *37*, 157–167.
Sibson, R. H. (2003), Thickness of the seismic slip zone, *Bull. Seismol. Soc. Am.*, *93*(3), 1169–1178.
Sims, J. (1993), Chronology of displacement on the San Andreas fault in central California: Evidence from reversed positions of exotic rock bodies near Parkfield, California, in *The San Andreas Fault System: Displacement, Palinspastic Reconstruction and Geologic Evolution*, *Geol. Soc. Am. Mem.*, vol. 178, edited by R. E. Powell, R. J. Weldon, and J. C. Matti, pp. 231–256.
Smith, S. A., A. Bistacchi, T. M. Mitchell, S. Mittempergher, and G. Di Toro (2013), The structure of an exhumed intraplate seismogenic fault in crystalline basement, *Tectonophysics*, *599*, 29–44.
Soliva, R., and A. Benedicto (2004), A linkage criterion for segmented normal faults, *J. Struct. Geol.*, *26*(12), 2251–2267.
Stirling, M. W., S. G. Wesnousky, and K. Shimazaki (1996), Fault trace complexity, cumulative slip, and the shape of the magnitude-frequency distribution for strike-slip faults: A global survey, *Geophys. J. Int.*, *124*, 833–868, doi:10.1111/j.1365-246X.1996.tb05641.x.
Tapponnier, P., and P. Molnar (1979), Active faulting and Cenozoic tectonics of the Tien Shan, Mongolia and Baikal regions, *J. Geophys. Res.*, *84*, 3425–3459, doi:10.1029/JB084iB07p03425.
Tinti, E., P. Spudich, and M. Cocco (2005), Earthquake fracture energy inferred from kinematic rupture models on extended faults, *J. Geophys. Res.*, *110*, B12303, doi:10.1029/2005JB003644.
Valoroso, L., L. Chiaraluce, D. Piccinini, R. Di Stefano, D. Schaff, and F. Waldhauser (2013), Radiography of a normal fault system by 64,000 high-precision earthquake locations: The 2009 L'Aquila (central Italy) case study, *J. Geophys. Res. Solid Earth*, *118*, 1156–1176, doi:10.1002/jgrb.50130.
Valoroso, L., L. Chiaraluce, and C. Collettini (2014), Earthquakes and fault zone structure, *Geology*, *42*, 343–346, doi:10.1130/G35071.1.
Vermilye, J. M., and C. H. Scholz (1998), The process zone: A microstructural view of fault growth, *J. Geophys. Res.*, *103*(B6), 12,223–12,237, doi:10.1029/98JB00957.
Vermilye, J. M., and C. H. Scholz (1999), Fault propagation and segmentation: Insight from the microstructural examination of a small fault, *J. Struct. Geol.*, *21*(11), 1623–1636.
Viegas, G., R. E. Abercrombie, and W. Y. Kim (2010), The 2002 *M*5 Au Sable Forks, NY, earthquake sequence: Source scaling relationships and energy budget, *J. Geophys. Res.*, *115*, B07310, doi:10.1029/2009JB006799.
Walsh, J. J., and J. Watterson (1988), Analysis of the relationship between displacements and dimensions of faults, *J. Struct. Geol.*, *10*(3), 239–247.
Walsh, J. J., J. Watterson, W. R. Bailey, and C. Childs (1999), Fault relays, bends and branch-lines, *J. Struct. Geol.*, *21*(8), 1019–1026.
Walsh, J. J., W. R. Bailey, C. Childs, A. Nicol, and C. G. Bonson (2003), Formation of segmented normal faults: A 3-D perspective, *J. Struct. Geol.*, *25*(8), 1251–1262.
Wechsler, N., Y. Ben-Zion, and S. Christofferson (2010), Evolving geometrical heterogeneities of fault trace data, *Geophys. J. Int.*, *182*(2), 551–567.
Wegler, U., H. Nakahara, C. Sens-Schönfelder, M. Korn, and K. Shiomi (2009), Sudden drop of seismic velocity after the 2004 M_w 6.6 mid-Niigata earthquake, Japan, observed with passive image interferometry, *J. Geophys. Res.*, *114*, B06305, doi:10.1029/2008JB005869.
Wesnousky, S. G. (1988), Seismological and structural evolution of strike-slip faults, *Nature*, *335*(6188), 340–342, doi:10.1038/335340a0.
Wesnousky, S. G. (2008), Displacement and geometrical characteristics of earthquake surface ruptures: Issues and implications for seismic-hazard analysis and the process of earthquake rupture, *Bull. Seismol. Soc. Am.*, *98*(4), 1609–1632.
Willemse, E. J., and D. D. Pollard (1998), On the orientation and patterns of wing cracks and solution surfaces at the tips of a sliding flaw or fault, *J. Geophys. Res.*, *103*(B2), 2427–2438, doi:10.1029/97JB01587.
Willson, J. P., R. J. Lunn, and Z. K. Shipton (2007), Simulating spatial and temporal evolution of multiple wing cracks around faults in crystalline basement rocks, *J. Geophys. Res.*, *112*, B08408, doi:10.1029/2006JB004815.
Yang, H., and L. Zhu (2010), Shallow low-velocity zone of the San Jacinto fault from local earthquake waveform modelling, *Geophys. J. Int.*, *183*(1), 421–432.
Yang, H., L. Zhu, and E. S. Cochran (2011), Seismic structures of the Calico fault zone inferred from local earthquake travel time modelling, *Geophys. J. Int.*, *186*(2), 760–770.
Yang, W., Z. Peng, B. Wang, Z. Li, and S. Yuan (2015), Velocity contrast along the rupture zone of the 2010 M_w6.9 Yushu, China, earthquake from fault zone head waves, *Earth Planet. Sci. Lett.*, *416*, 91–97.
Zhang, P.-Z., X.-Z. Wen, Z.-K. Shen, and J.-H. Chen (2010), Oblique, high-angle, listric-reverse faulting and associated development of strain: The Wenchuan earthquake of May 12, 2008, Sichuan, China, *Annu. Rev. Earth Planet. Sci.*, *38*, 353–382.
Zigone, D., Y. Ben-Zion, M. Campillo, and P. Roux (2015), Seismic tomography of the Southern California plate boundary region from noise-based Rayleigh and Love waves, *Pure Appl. Geophys.*, *172*(5), 1007–1032.